

Combined Optical and Radio-Frequency Measurements of a Lightning Megaflash by the FORTE Satellite

Michael Jay Peterson¹, Tracy Ellen Lavezzi Light², and Xuan-Min Shao²

¹ISR-2, Los Alamos National Laboratory

²Los Alamos National Laboratory (DOE)

November 24, 2022

Abstract

The optical and VHF instrumentation on the FORTE satellite is used to document the combined phenomenology evolution of a lightning “megaflash” - mesoscale lightning that propagates laterally over exceptional distances. We identify a FORTE flash whose maximum extent was 82 km and inferred length over multiple distinct branches exceeded 100 km. This flash lasted 1.2 s and produced 250 optical and 591 RF events. We find that the channel development mapped by FORTE’s pixelated lightning imager (LLS) occurred at a typical speed of 2.6×10^5 m/s and was accompanied by sustained periods VHF emission that could individually exceed 100 ms in duration. The impulsive IC events generated by the flash indicate that this development occurred at altitudes between 3 and 8 km. Four +CG strokes were identified in the VHF waveform data that are responsible for two of the three highly-radiant LLS groups (the third radiant group came from a possible -CG while 2 of the +CGs were not as optically bright as the others). These strokes occurred at different locations throughout the flash footprint with the most distant strokes separated by approximately 50 km. These space-based observations match previous observations of megaflashes from space as well as ground-based measurements of slow negative leader development during “spider” lightning, suggesting that FORTE is sensing the same phenomena.

1 **Combined Optical and Radio-Frequency Measurements**
2 **of a Lightning Megaflash by the FORTE Satellite**

3
4 **Michael Peterson¹, Tracy E. L. Light¹, Xuan-Min Shao¹**

5
6
7 ¹ISR-2, Los Alamos National Laboratory, Los Alamos, New Mexico

8
9
10
11
12 Corresponding author: Michael Peterson (mpeterson@lanl.gov), B241, P.O. Box 1663 Los
13 Alamos, NM, 87545

14
15
16 **Key Points:**

- 17 • Combined FORTE optical / RF instrumentation document the evolution of a mesoscale
18 oceanic lightning “megaflash”
- 19 • Optical observations reveal the development of long horizontal lightning channels that
20 extended over 82 km
- 21 • RF observations indicate substantial leader activity accompanying channel development
22 as well as 4 distinct +CG strokes spread throughout the flash area

23 **Abstract**

24

25 The optical and VHF instrumentation on the FORTE satellite is used to document the
26 combined phenomenology evolution of a lightning “megaflash” – mesoscale lightning that
27 propagates laterally over exceptional distances. We identify a FORTE flash whose maximum
28 extent was 82 km and inferred length over multiple distinct branches exceeded 100 km. This
29 flash lasted 1.2 s and produced 250 optical and 591 RF events. We find that the channel
30 development mapped by FORTE’s pixelated lightning imager (LLS) occurred at a typical speed
31 of $2.6 \times 10^5 \text{ m s}^{-1}$ and was accompanied by sustained periods VHF emission that could
32 individually exceed 100 ms in duration. The impulsive IC events generated by the flash indicate
33 that this development occurred at altitudes between 3 and 8 km. Four +CG strokes were
34 identified in the VHF waveform data that are responsible for two of the three highly-radiant LLS
35 groups (the third radiant group came from a possible -CG while 2 of the +CGs were not as
36 optically bright as the others). These strokes occurred at different locations throughout the flash
37 footprint with the most distant strokes separated by approximately 50 km. These space-based
38 observations match previous observations of megaflashes from space as well as ground-based
39 measurements of slow negative leader development during “spider” lightning, suggesting that
40 FORTE is sensing the same phenomena.

41

42 **Plain Language Summary**

43

44 Pixelated lightning imagers map the lateral development of lightning flashes by recording
45 how the locations of radiant pulses produced by lightning change over time. Most lightning
46 flashes measured by instruments including NASA’s Lightning Imaging Sensor (LIS) and
47 NOAA’s Geostationary Lightning Mapper (GLM) are small and repeatedly illuminate the same
48 cloud region with little apparent motion between pulses. However, certain thunderstorms are able
49 to produce “megaflashes” that start in one place and then develop up to hundreds of kilometers
50 horizontally from the initiation point. These propagating flashes pose a unique hazard because
51 they can strike the ground in places where lightning is not expected.

52 We use measurements from the FORTE satellite to investigate what radio-frequency
53 signals accompany the optical signatures of a lightning megaflash. RF data provide insights into
54 the physical origin of the optical lightning emissions. A detailed analysis of a megaflash 82 km
55 across reveals that optical flash propagation is accompanied by abundant VHF signatures of
56 leader development as well as multiple distinct +CG strokes at different places across the flash.

57

58 **1 Introduction**

59 Lightning generates optical signals by rapidly heating the air surrounding the lightning
60 channel. Temperatures along the channel may exceed 20,000 K (Prueitt, 1963), causing
61 ionization of the major atmospheric constituent gasses. The ionization, excitation, and
62 recombination of atmospheric constituents results in particularly strong optical emissions in the
63 near-infrared neutral oxygen and neutral nitrogen atomic lines. Optical pulses are produced by
64 Cloud-to-Ground (CG) strokes as well as a myriad of in-cloud processes that illuminate the
65 lightning channel.

66 Space-based lightning imagers such as NOAA's Geostationary Lightning Mapper (GLM:
67 Goodman et al., 2013) and NASA's Optical Transient Detector (OTD: Christian et al., 2003) and
68 Lightning Imaging Sensor (LIS: Christian et al., 2000; Blakeslee et al., 2014) report the spatial
69 and temporal evolution of individual flashes by measuring transient changes in cloud-top
70 illumination from the lightning discharges that comprise the flash. OTD, LIS and GLM record
71 the optical radiance in a narrow band centered on the neutral Oxygen line triplet at 777.4 nm to
72 take advantage of the emissions peak resulting from these underlying physical processes
73 (Christian et al., 2000; Goodman et al., 2010).

74 Optically bright lightning processes vary in terms of extent, speed, current, and polarity.
75 Identifying reliable optical signatures for specific processes such as strokes (Koshak, 2010) has
76 proven difficult because optical measurements provide little information on the nature of the
77 source beyond the intense heating along the channel, and also because the optical signals
78 recorded from space have been modified by scattering and absorption in the cloud medium
79 (Thomson and Krider, 1982; Koshak et al., 1994; Light et al., 2001a,b; Thomas et al., 2000;
80 Suszcynsky et al., 2000). Scattering causes the optical signals to be diluted in space and

81 broadened in time. Flashes that occur in particularly inhomogeneous clouds have their footprints
82 sculpted by spatial distribution of hydrometeors in the thundercloud (Peterson et al., 2017a).
83 Flashes that occur near a cloud boundary often take on an irregular shape as the radiance
84 measured from space follows the boundary (Peterson et al., 2017b), while dense convective cells
85 can produce “holes” in otherwise contiguous flash footprints by blocking light from reaching
86 orbit in sufficient quantities to trigger the instrument. Radiance can also reflect off the sides of
87 neighboring clouds or the tops of lower cloud decks to expand the flash footprint far beyond the
88 extent of the parent thunderstorm (i.e., Figure 1 in Peterson and Liu, 2013). Due to these
89 scattering effects, the optical signals recorded by OTD, LIS and GLM may contain as much
90 information about the cloud scene as they do about lightning.

91 Still, there are optical signatures in the lightning imager data that reveal key aspects of
92 the physical evolution of the lightning flash. Lateral propagation in the optical flash structure, for
93 example, indicates horizontal leader development (Peterson et al., 2018). LIS and GLM observe
94 both the flickering at the ends of developing lightning channels and the waves of radiant energy
95 retracing an established channel back to its origin that have been noted in ground-based
96 observations (Mazur et al., 1998; Winn et al., 2011). The optical pulses that map the
97 development of these flashes are small and relatively dim, so the shapes of their footprints (as
98 imaged by a lightning imager with kilometer-scale pixels) are not modified substantially by
99 scattering. Thus, the structure of propagating optical flashes measured by space-based lightning
100 imagers approximates a two-dimensional vertically-integrated view of the three-dimensional
101 flash structure that would be mapped by a Lightning Mapping Array (LMA: Rison et al., 1999).
102 The two key caveats with optical space-based lightning mapping are the large pixel footprints (4-
103 5 km for LIS and 8-14 km for GLM) and the decreasing source detection efficiency as the optical

104 thickness of the intervening cloud layer increases. Leader propagation through deep convection
105 that is routinely observed by LMAs (i.e., Lang et al., 2017) is generally not resolved from space.
106 As a result, the LIS / GLM measurements of flash extent are a minimum estimate for the scale of
107 lightning that mostly captures long horizontal channels in stratiform and anvil clouds (Peterson
108 and Liu, 2011).

109 We have used lightning imager data to measure the horizontal extent of propagating
110 flashes and to calculate their development speeds (Peterson et al., 2018). We have also defined
111 “series” features (Peterson et al., 2017b) to describe distinct periods of sustained optical emission
112 that typically accompany widespread branching and recoil waves, but can also capture lightning
113 emissions related to gigantic jets (Boggs et al., 2019) and return stroke continuing currents
114 (Bitzer, 2017). Peak optical emissions during individual series are also used to define an optical
115 multiplicity that describes how often flashes light up well above the numerous low-radiance
116 pulses associated with cloud discharges (Peterson and Rudlosky, 2019). The optical multiplicity
117 is advanced by strokes as well as K-changes that both produce strong emission along the
118 channel.

119 While these optical-only capabilities are useful for analyzing lightning activity, a
120 comprehensive view of lightning physics is achieved when optical and RF measurements are
121 combined to describe the same flash. We previously used coincident optical and VHF
122 measurements taken by the Fast On-Orbit Recording of Transient Events (FORTE) satellite to
123 identify the physical processes responsible for the optical signals recorded by its pixelated
124 lightning imager during a hybrid CG flash (Peterson et al., 2020a). In this study, we use the same
125 approach to investigate the combined-phenomenology evolution of a horizontally-expansive
126 lightning megaflash observed over the open ocean near the Canary Islands.

127

128 **2 Data and Methodology**

129 The FORTE satellite was a unique platform for examining lightning from space because
130 it contained both optical and RF payloads for observing transient lightning pulses, and because
131 its instrumentation was operated in campaign mode. The optical / RF trigger settings, data record
132 lengths, and RF frequency bands were periodically reconfigured on-orbit over the FORTE
133 mission. FORTE thus provides multiple different types of coincident data that can be used to
134 assess various aspects of lightning discharges. A detailed description of the FORTE RF payloads
135 is provided in Jacobson et al. (1999), while the optical payloads are described in Suszcynsky et
136 al. (2000, 2001). Moreover, the FORTE mission and its key scientific findings are reviewed in
137 Light (2020). The sections below summarize the RF and optical payload configurations that
138 pertain to our megaflash case of interest.

139 2.1 The FORTE Optical Lightning System

140 The optical payload on FORTE was known as the Optical Lightning System (OLS). The
141 OLS consisted of two different optical instruments. A high-speed photodiode detector recorded
142 broadband (0.4 μm – 1.1 μm) lightning pulses in 2 – 6 ms records with a 15 μs sampling interval.
143 The PDD could be triggered by optical lightning pulses anywhere within its 80° field of view. If
144 we think of the PDD as a single-pixel lightning imager, then it would have an effective frame
145 rate of 66,667 FPS. In both Peterson et al. (2020a) and this study, the PDD was configured to
146 trigger autonomously and produce 1.92 ms records of optical lightning activity. The PDD had a
147 dead time between records that was approximately equal to the record length. Thus, we will see
148 ~2 ms gaps between the PDD records from successive triggers during periods of sustained

149 optical emission. We also noted in Peterson et al. (2020a) that the PDD stops reporting after a
150 specific number of triggers on flash time scales. As the megaflash case occurred around the same
151 time as the previous hybrid CG flash case, this 20-trigger maximum will be a limitation in the
152 present study as well.

153 The second OLS instrument was a pixelated lightning imager known as the Lightning
154 Locating System (LLS). The LLS consisted of the same front-end optical assembly and fixed-
155 position CCD focal plane assembly used by LIS that was provided by NASA Marshall Space
156 Flight Center, and an operations and signal processing module designed by Sandia National
157 Laboratories. The LLS was designed to have a lower (405 FPS) frame rate than LIS (500 FPS).
158 The key role of the LLS was to geolocate lightning sources. Coordinated observations with the
159 PDD would then enable light curves to be resolved at orders of magnitude finer time scales than
160 LLS or LIS could measure.

161 Because the LLS signal processing module was designed by Sandia, the artifact filters
162 and cluster feature algorithm developed for LIS (Christian et al., 2000) were not applied to the
163 LLS data during the FORTE mission. LLS observations in its standard operating mode include
164 only pixel-level “event” detections. Events are recorded whenever the measured radiance in a
165 given CCD pixel during a single 2.47-ms integration frame exceeds a noise-riding threshold
166 above the radiance of the background scene. Note that this description of events follows the
167 NASA terminology. The raw LLS events (subsequently termed “super-events” because they are
168 conceptually similar to the proposed concept of “supergroups” in Tillier et al., 2019) can
169 describe the same pixel being illuminated for multiple frames. For consistency with the other
170 sensors such as LIS, we extract the single-frame pixel detections from the raw LLS super-events
171 and use the standard term “events” to describe them. Artifacts are handled by simply ignoring

172 subsequent detections from the same pixel once events are recorded in that pixel during two
173 adjacent integration frames. This filter prevents the LLS from measuring sustained optical
174 emission from a stationary source (i.e., continuing current with a return stroke), but still permits
175 the LLS to record sustained emission from propagating sources (i.e., lateral flash development,
176 K-waves).

177 2.2 The FORTE Radio Frequency (RF) System

178 The Radio Frequency (RF) system was comprised of three broadband receivers
179 connected to the two identical Log-Periodic Antennas (LPAs) mounted along FORTE's 10-m
180 nadir-pointing boom. The three receivers were divided between two RF payloads known as
181 TATR and HUMR. TATR consisted of 2 independent RF receivers (TATR/A and TATR/B) that
182 could each be tuned to measure one of the FORTE antennas over a 22-MHz subband. The record
183 lengths and the ratio of pretrigger to posttrigger data could also be configured. HUMR,
184 meanwhile, sampled a wider (85 MHz) band over longer records that typically lasted 3 ms.

185 This study and Peterson et al. (2020a) both use TATR observations from late 1999 when
186 it was configured to record lowband (26 – 48 MHz) waveforms and set to trigger autonomously.
187 In its autonomous mode, TATR monitored the RF power in eight RF channels that were each 1-
188 MHz wide. Whenever the received power exceeded the noise-riding background value in one of
189 these channels by a certain threshold, the instrument would report an alarm. Triggers require
190 multiple simultaneous alarms in the 8 channels, and the number of alarms required to trigger the
191 instrument and report an event was a commandable parameter. Typically, only RF events that
192 triggered 5 of the 8 channels are examined (i.e., Jacobson et al., 2000), but we instead consider

193 all TATR triggers during a time window encompassing LLS flashes (± 330 ms) in order to
194 capture the weakest lightning phenomena detectable from orbit.

195 While optical lightning signals are modified by scattering in the cloud, VHF pulses are
196 modified by the ionospheric plasma between the source and satellite. Ionospheric dispersion
197 causes a frequency-dependent group delay in the recorded VHF pulses. Signals on the low-
198 frequency side of the band arrive after the high-frequency signals, and the waveforms appear
199 “chirped” (Jacobson et al., 2000). The severity of the dispersion depends on the Total Electron
200 Content (TEC) of the ionospheric slant path between the source and sensor. By fitting the
201 dispersion in the received signal to a physics-based mathematical model, we can “dechirp” the
202 data and align the VHF waveforms to their vacuum time of arrival. The dechirping process also
203 yields an estimate for the ionospheric TEC encountered by the signals along their slant path
204 through the ionosphere, which we can further use to identify signals that come from elsewhere in
205 the FORTE field of view (Jacobson et al., 1999).

206 Unlike in the hybrid CG case in Peterson et al. (2020a), we find no evidence that
207 thunderstorms located at different slant angles are contributing TATR triggers during the
208 duration of the megaflash considered here. However, there is one TATR trigger in the flash that
209 resulted from an on-board discharge. This trigger was a single impulsive event that produced the
210 strongest peak RF power over the flash duration, but had no evidence of ionospheric dispersion
211 in the event waveform data. This on-board discharge event is preserved in the RF waveform
212 records to show how these features contaminate natural lightning signals, but it is otherwise
213 ignored in the broader discussion of the flash.

214 2.3 FORTE combined-phenomenology lightning cluster data

215 Though flash cluster data was not created from the LLS events during the FORTE
216 mission, the LIS (Christian et al., 2000) and GLM (Goodman et al., 2010) flash cluster
217 algorithms have been documented in the literature and can be adapted for use with FORTE. We
218 used the GLM algorithm as the basis for constructing a combined-phenomenology lightning
219 cluster feature dataset in Peterson et al. (2020a) that includes both optical and RF features.

220 Design considerations for the full FORTE cluster feature dataset are described at length
221 in Peterson et al. (2020a) and we will discuss only the optimal data structure for FORTE
222 analyses here (shaded boxes in Table 1 from Peterson et al., 2020a). LLS events are used to
223 define “group” features that represent contiguous regions on the LLS CCD array that are lit up
224 during the same 2.47-ms integration frame. Groups are then clustered into LLS “flashes” using
225 the same Weighted Euclidian Distance (WED) model as LIS / GLM. The distance and time
226 thresholds for assigning two groups to the same flash are 16.5 km and 330 ms, respectively. If a
227 new group occurs that could belong to multiple flashes, a “full fit” matching technique is
228 employed that merges the two candidate flashes into a single flash cluster. “Series” features are
229 also constructed that describe sustained optical emission within individual flashes. Series
230 encompass all groups in a given flash that occur either sequentially or following a 1-frame gap.
231 Finally, thunderstorm areas of interest (or “areas”) are constructed by applying the WED model
232 to the flash cluster data with the same 16.5 km distance threshold and no time threshold (though
233 all flashes in the same area should occur during the same FORTE orbit).

234 The FORTE PDD and RF data are ingested into the LLS hierarchy at the event level after
235 making a minor change to the “event” definition. In the LIS / GLM literature, an event is defined
236 as a single triggered pixel on the CCD array during an integration frame. We slightly generalize
237 this definition to describe an event as a unique trigger during the millisecond-scale triggering

238 interval associated with the instrument. The PDD and RF system can have only one unique
239 trigger from their FOVs at a given instant, while the LLS would have a unique trigger for each
240 pixel that lights up in a given frame. With this change, we can construct lightning cluster feature
241 data structures (i.e., areas, flashes, groups) for the PDD and RF system that parallel the LLS
242 hierarchy. The high sampling rates of these instruments also allow us to extend the data tree to
243 finer time scales that occur within a single “event.” We define “pulses” as features describing
244 periods of sustained emission above a noise-riding background threshold that occur within a
245 single event record. We also define “samples” as single calibrated measurements at the native
246 sampling rate of the instrument. Events are the parents of pulses and the grandparents of
247 samples. We finally integrate the LLS, PDD, and RF features by defining “step-parent”
248 relationships that assign PDD and RF events, pulses, and samples to LLS groups, series, flashes,
249 and areas.

250

251 **3 Results**

252 The present study aims to investigate the RF signatures that accompany lateral
253 propagation in the optical lightning imager data. In particular, we will be focusing on the large-
254 scale propagation that we see with megaflashes where the lateral development is widespread and
255 organized along multiple distinct branches. LMA networks have mapped extensive propagating
256 flashes that measure 321 km from one end to the other (Lang et al., 2017), while GLM has
257 recorded cases that exceed 500 km in length (Peterson, 2019c; Lyons et al., 2019). The most
258 exceptional megaflash cases recognized as lightning extremes by the World Meteorological

259 Organization (WMO) are now two different cases of GLM flashes that reached 709 km in extent
260 and 16.73 s in duration, respectively (Peterson et al., 2020b).

261 The common aspect shared by all of these exceptional megaflash cases is that they
262 primarily develop through the electrified stratiform region of a large (mesoscale) mature or
263 dissipating storm system. Stratiform clouds become electrified through a combination of the
264 advection of charged ice particles from the convective core (Carey et al., 2005) and in-situ
265 charging in the radar bright band (Rutledge and MacGorman, 1988) that may be enhanced by
266 local mesoscale updrafts (Ely et al., 2008; Lang and Rutledge, 2008). These processes generate
267 multiple vertically-thin charge layers that can extend laterally over hundreds of kilometers
268 (Marshall and Rust, 1993; Stolzenburg et al., 1994; Lang et al., 2004; Marshall et al., 2009) and
269 act a conduit for lightning propagation.

270 The combined optical and RF phenomenology of complex horizontally-propagating
271 “spider” lightning was studied from the ground in Mazur et al. (1998) using a whole sky
272 intensified camera system co-located with a VHF interferometer. They concluded that spider
273 lightning consists of slow ($2\text{-}4 \times 10^5 \text{ m s}^{-1}$) negative leaders that produce transient optical pulses
274 at the tips of the branching channels and occasional continuous illumination along the entire
275 channel resulting from sustained current flow that may last tens to hundreds of milliseconds.
276 Because the development speeds, VHF signatures, and flickering at the ends of branches in the
277 optical measurements are all similar to stepped-leaders in negative CG flashes, they suggested
278 that spider lightning results from the same underlying physical processes.

279 The FORTE satellite is equipped to make similar optical and VHF measurements of
280 horizontally-propagating lightning to Mazur et al. (1998) from space. FORTE observations have

281 an expanded horizontal domain compared to the range from a single site to the local horizon, and
282 its orbital measurements are mapped in geographic coordinates rather than spherical coordinates
283 surrounding the site. Thus, we do not have to assume an altitude for the lightning channels to
284 compute lateral distance or propagation speed. However, the key limitation to observing
285 megaflashes with FORTE is the short view times over a given thunderstorm (on the order of
286 minutes) due to its low Earth orbit. The FORTE satellite would have to be in the right place at
287 the right time to see a megaflash – and this is why megaflashes are rarely observed in the OTD /
288 LIS records. The FORTE LLS has detected a small number of megaflashes whose extents are <
289 100 km, but whose total lengths are considerably larger. In the following sections, we will
290 examine the longest of these LLS megaflash cases in detail.

291 3.1 Overview of FORTE measurements during an oceanic megaflash on 12/3/1999

292 Megaflash cases are identified in the FORTE record according to the maximum great
293 circle distance between LLS groups. This is a low estimate of flash scale because megaflashes do
294 not propagate directly from one end to the other, but instead take a meandering path through the
295 electrified cloud. Peterson et al. (2018) attempted to measure total flash length by constructing
296 skeleton images of the two-dimensional flash structure reported by LIS and found that flash
297 length was usually 2-3 times greater than its reported extent.

298 The top LLS flash in terms of extent occurred over the Atlantic Ocean between the
299 Canary Islands and the Azores on 12/3/1999 at 22:30:22 UTC (23:30:22 local time in Santa Cruz
300 de Tenerife). It was 82 km across and produced 69 LLS series, 98 LLS groups, and 230 LLS
301 events over a duration of 1180 ms. In total, it illuminated a cloud-top area of 5203 km² with the

302 largest group in the flash illuminating 2386 km² of cloud. In addition to these LLS triggers, the
303 PDD contributed 20 optical events and TATR recorded 591 VHF events.

304 The LLS Flash Extent Density (FED: Lojou and Cummins, 2004) plotted in Figure 1a
305 indicates that the flash rate for the storm was low (3 flashes in 15 minutes), and that there were
306 no intense thunderstorms nearby that could have contributed the large number of TATR triggers
307 during the flash duration. The trigger rates in Figure 1b show that there was only 1 isolated
308 optical trigger in the minute leading up to the flash and that subsequent triggers after the flash
309 occurred more than 1 s following the final LLS group. Unlike the hybrid CG case in Peterson et
310 al. (2020a), this case did not contain any RF triggers before first LLS light or after final light.

311 3.2 Evolution of optical signals from the megaflash

312 Figure 2 documents the overall evolution of the LLS flash. The central panel (Figure 2c)
313 shows the plan view of the events and groups in the flash. Normalized event energies from each
314 pixel on the CCD array are summed to produce a color contour plot representing the spatial
315 radiance distribution. The progression of groups is traced in time with line segments that connect
316 each group centroid to its nearest preceding group. The greyscale color palette denotes the
317 sequential group index from dark (first group) to light (final group), and is standardized between
318 all panels in Figure 2. Figure 2a shows the longitudinal extent of all groups in the flash while
319 Figure 2d shows their latitudinal extents. Figure 2b displays a histogram of group energy
320 presented as a sigma level (the number of standard deviations above or below the mean for all
321 groups in the flash). Figure 2e and f, finally, show timeseries of group area and normalized
322 group energy.

323 The flash began along the southwestern flank of its footprint (Figure 2c) and propagated
324 to the northeast. At least 6 primary branches spanning more than 20-km (~2 pixels) can be noted
325 in the group-level structure that contain smaller features propagating laterally off the main
326 channels. The LLS groups associated with this lateral development are typically dim and small
327 ($100 - 200 \text{ km}^2$ in Figure 2e) – yet they account for the clear majority of optical triggers from the
328 flash. Only 3 groups reach the +1-sigma level (Figure 2b). We use the 1-sigma group count to
329 define an optical multiplicity parameter that quantifies how often a given flash lights up beyond
330 the baseline radiance from these common dim cloud pulses under the specific viewing conditions
331 of the flash. The optical multiplicity for this flash would thus be 3, with intervals of 43 ms and
332 311 ms separating the series containing these bright groups. The FORTE megaflicker considered
333 in this study produced groups that reached an exceptional 8-sigma above the average group
334 energy for the flash.

335 3.3 Combined optical and RF assessment of flash evolution

336 The timeseries in Figure 3 show the combined-phenomenology evolution of the LLS
337 flash. Optical group energies are plotted in Figure 3a for LLS and Figure 3b for PDD and are
338 normalized to the peak received group energy for each instrument on a logarithmic scale. TATR
339 event records are dechirped and “prewhitened” (to remove narrowband carrier waves), and then
340 the band-averaged peak VHF power for each trigger is shown in Figure 3c. Like the optical
341 energy, RF power is normalized relative to the strongest emissions during the flash window. The
342 TATR pulses recorded in each event are categorized as isolated impulses (single pulse), isolated
343 pulse pairs (single pair of pulses representing an IC source with a ground reflection), pulse trains
344 (multiple pulse pairs per TATR record), or diffuse / mixed pulses (broad pulses that may include
345 superimposed impulsive features). TATR records that do not contain any classifiable pulses are

346 designated “sustained featureless emission.” We divide the flash duration into 2-ms bins
347 (comparable in scale to PDD records or LIS / GLM groups) and then compute the fractions of
348 each pulse type per bin in Figure 3d.

349 Because we know the geographic position of the flash from the LLS observations, we can
350 compute the altitude of impulsive IC sources using the satellite position and the time delay
351 between pulses in each Trans-Ionospheric Pulse Pair (TIPP: Holden et al., 1995). Estimated
352 altitudes for the isolated impulsive IC events and pulse trains from Figure 3d are shown in Figure
353 3e. Finally, Figure 3f integrates the received optical LLS energy and TATR antenna response (in
354 $V^2 m^{-2}$) to compare the accumulation of optical / RF signals over the duration of the flash.

355 In our previous -CG case (Peterson et al., 2020a), the TATR triggers were intermittent
356 and dominated by impulsive IC events and K-changes. Leader activity ahead of the return stroke
357 produced sustained featureless emission that strengthened over multiple TATR records as the
358 stepped leader developed towards the surface and then a single strong VHF pulse occurred upon
359 seawater attachment. The TATR records in the current megaflash case, by contrast, are
360 dominated by periods of sustained featureless VHF emission over tens to hundreds of
361 milliseconds (Figure 3d). The longest-lasting TATR series feature started 200 ms into the LLS
362 flash and then persisted for 169 ms. Of the total 591 TATR events, 516 were classified as
363 sustained featureless emission. The remaining 75 TATR records contained 38 TIPPs, 38 diffuse
364 pulses, and 5 isolated single impulses (including one from the on-board discharge mentioned
365 previously). Note that the total number of pulses is greater than the number of events due to
366 certain events containing multiple pulses.

367 As with the energy budget from previous -CG flash in Peterson et al. (2020a), optical
368 energy from the megaflash accumulated rapidly in 1-2 frame increments in Figure 3f, while the
369 RF signals accumulated gradually over longer time intervals. The three high-radiance groups in
370 the LLS flash that exceeded the 1-sigma level contributed 5%, 30%, and 17% of the total energy
371 of the flash (total: 52%). The remaining 95 groups contributed 48% of the total energy.

372 While most TATR waveform records appear to originate from IC sources, four TATR
373 events contained the signatures of positive-polarity CG strokes described in Light et al. (2001b).
374 A spectrogram for the first of these strokes (at 14 ms into the LLS flash) is shown in Figure 4.
375 +CG events have a quick onset typically followed by a broad VHF pulse due to considerable in-
376 cloud activity following attachment. This lingering tail can last for tens of milliseconds, spanning
377 multiple TATR records. Mazur et al. (1998) noted comparable behavior from the ground in their
378 analysis of +CGs in spider lightning.

379 The other +CGs in the FORTE megaflash occur at 282 ms, 335 ms, and 592 ms into the
380 LLS flash with similar TATR records to the spectrogram shown in Figure 4. The key difference
381 with these later +CGs is that they occurred under a stronger RF background from the widespread
382 leader activity in the later stages of the flash. We use these RF signatures to divide the flash into
383 4 phases: initial horizontal development of the lightning channel and first +CG stroke (0 ms to
384 265 ms), peak optical emission during the second +CG stroke followed by weaker emission
385 during the third +CG (265 ms to 400 ms), further branching along the northern flash extent
386 leading up to the fourth +CG stroke (400 ms to 700 ms), and then final optical activity after the
387 continuous VHF emission ceased (700 ms to 1180 ms). The evolution of the flash during these
388 phases is discussed below.

389

390 **4 Discussion**

391 4.1 Initial horizontal development of the lightning channel and first +CG stroke

392 An evolution plot for the first optical / RF events in the flash is shown in Figure 5. The
393 key difference between the format of Figure 3 and Figure 5 is that the group area timeseries is
394 removed and a TATR RF power timeseries is displayed in its place. PDD sample energies are
395 also plotted in blue alongside the normalized LLS group energies in Figure 5e. The LLS flash
396 began with a single-pixel event at $t = 0$ ms that has slightly less than 1% of the optical energy of
397 the most radiant group in the flash. The baseline for single-pixel detections is $\sim 0.7\%$ to 1% of
398 peak emission. These optical emissions from individual LLS pixels were too faint / localized for
399 the PDD to trigger.

400 The first 2 TATR events were recorded 4 ms and 14 ms into the LLS flash. The first
401 TATR event consisted of an impulsive IC TIPP with additional IC pulse pairs embedded in the
402 VHF background. Unlike Peterson et al. (2020a), this flash did not start with a powerful TIPP
403 waveform from a Narrow Bipolar Event (NBE). Any IC events that could have occurred before
404 first LLS light were too weak to trigger TATR.

405 The first +CG stroke occurred 14 ms after the first LLS event and 10 ms after the first
406 TATR event. The first long period of continuous RF triggering occurred following this stroke
407 (Figure 5f). During this time, two impulsive IC events were noted at ~ 5 km altitude as well as an
408 isolated single impulse. This single-peak event at 22 ms was caused by the on-board discharge
409 noted previously. The remaining TATR triggers from 14 ms to 41 ms were all diffuse featureless

410 emission associated with leader activity. The PDD triggered continuously over this period,
411 demonstrating that there was sustained optical emission accompanying the continuous VHF
412 activity. The LLS only triggered twice, however, with a 5-pixel group at 14 ms and a single-pixel
413 group at 24 ms. The optical energies in all lit-up pixels were near the minimum for the flash
414 (Figure 5c), suggesting that the emissions that triggered the PDD were spread over a large area
415 with energy densities only occasionally exceeding the LLS detection threshold in its individual
416 pixels.

417 The continuous TATR triggering stops at 41 ms and then there is a lull with only 2 TATR
418 triggers (one IC pulse train at 4.2 km altitude and one sustained featureless emission) until 112
419 ms into the LLS flash. The time period from 112 ms until 215 ms depicted in Figure 6 describes
420 the incremental development of the flash to the north and east through small / dim groups
421 illuminating the tips of the extending branches. RF activity is intermittent before 200 ms and
422 evenly distributed between IC pulse pairs / trains from sources at 6 km altitude and sustained
423 featureless emission. The LLS and PDD trigger simultaneously at 157 – 160 ms following a
424 pulse train with a relatively weak peak RF power, and the PDD continues to trigger until its 20
425 triggers are exhausted by 210 ms.

426 TATR began its longest period of continuous triggering at 200 ms. Unlike the previous
427 continuous period, it did not begin with a stroke. The PDD recorded sustained emissions starting
428 at 160 ms. The remainder of the initial IC lateral development phase from 230 ms until 265 ms is
429 shown in Figure 7. The first LLS groups at 235 ms resulted from the tips of all existing channels
430 being simultaneously illuminated. Then the first 1-sigma bright group is detected during the next
431 integration frame (starting at 238 ms) where nearly the entire extent of the main channel lit up at
432 once. VHF waveform analysis of what caused this behavior is inconclusive, as the high VHF

433 background obscures portions of the waveforms that are important for pulse characterization.
434 Figure 3d shows that sustained featureless VHF emission accompanied the first 1-sigma LLS
435 group. However, a detailed analysis of the TATR waveforms found a single narrow peak in the
436 TATR trigger at 235 ms consistent with a -CG. This peak is so poorly resolved that the
437 automated dechirp algorithm fails to find it - causing no TEC estimate to be returned and the
438 event to be labeled as sustained featureless emission.

439 We do not see the increasing VHF emission leading up to attachment that typically
440 accompanies -CGs in the event recorded at 235 ms, as it would be buried in the high VHF
441 background. Furthermore, the peak occurred at the end of the TATR record due to the
442 continuous TATR triggering. Thus, we cannot be certain that this was a single solitary peak from
443 a -CG. An alternate explanation could be that it was an impulsive IC event where the second
444 peak in the TIPP occurred during the dead time between TATR records. Of these two
445 possibilities, the strong optical emission accompanying the event suggests that the -CG
446 explanation is more likely - but this is not assured.

447 The subsequent groups over the next 20 ms were all located along the main channel and
448 constituted one of the longest-lasting LLS series features in the flash (15 ms in duration). These
449 factors seem to indicate a sustained flow of current down the channel that is only partially
450 resolved in the pixelated LLS data. PDD data would be required to confirm continuous optical
451 emission (as with the first +CG). The maximum group separation by 260 ms was 68 km, and this
452 lateral development allows us to infer an average propagation speed $2.6 \times 10^5 \text{ m s}^{-1}$.

453 The development of this FORTE flash is consistent with the ground-based observations
454 of spider lightning from Mazur et al. (1998). We find pulses illuminating the tips of branched

455 channels in the flash and luminosity along the channel that may have been sustained for many
456 milliseconds in agreement with their video observations. The lateral development speed of our
457 flash also fits within their $2\text{-}4 \times 10^5 \text{ m s}^{-1}$ range for the slow negative leaders that occur in spider
458 lightning events, while the sustained RF emission recorded by TATR also agrees with their RF
459 records of strong continuous VHF radiation from the slow leader (Figure 12 and 13 in Mazur et
460 al., 1998). Unlike the previous ground-based results, the FORTE LLS did not map lightning
461 activity that was distinct from the propagating spider event. If additional fast negative leaders or
462 positive leaders occurred in other parts of the lightning “tree” as described in Mazur et al. (1998),
463 they were either too weak to be resolved from space or co-located with the geographic extent of
464 the developing spider flash.

465 4.2 Optical emission during second and third +CG strokes

466 The most radiant group in the flash (8-sigma) occurred at 282 ms in the evolution plot in
467 Figure 8. This was the second bright group (> 1 -sigma) in the flash, with the first describing the
468 illumination of the long horizontal channel during a possible -CG. The RF power coincident with
469 this second bright group increased rapidly by 10 dB and then fell back to the average sustained
470 RF power level over a period of 12 ms – conforming to the +CG signature that we saw with the
471 first stroke in Figures 4 and 5. The long-duration VHF activity following the stroke (also seen in
472 the +CG strokes in Mazur et al., 2008) is interesting because it was not noted in the TATR
473 waveforms from Light et al. (2001b), where the “normal” (i.e., non-megaflash) +CG pulses were
474 shown to last between $\sim 150 \mu\text{s}$ and $500 \mu\text{s}$.

475 This behavior may be a unique feature of VHF emission from megaflashes that can
476 access charge from throughout their vast networks of ionized lightning channels during strokes

477 and funnel it to the surface. We see evidence for this in the LLS data from this second +CG. This
478 second +CG stroke was located along the northeastern flank of the flash. If we assume that the
479 strokes are co-located with the centroid of the brightest simultaneous LLS groups, then the first
480 and second +CG strokes were separated by approximately 50 km. However, the 8-sigma bright
481 group is not the only LLS activity during the second +CG. Two single-pixel groups occurred
482 during the VHF tail that appear to extend the existing channel: one at the flash origin, and one on
483 the eastern flank of the flash south of the second +CG (though, still within the cloud-region that
484 the stroke illuminated two frames prior). This indicates that the whole 60-km channel was active
485 during this stroke, with these new breakdowns contributing to the VHF tail. It is likely that the
486 channel was continuously illuminated (as we saw with the PDD waveforms during the first
487 stroke), but that LLS only triggered intermittently in the pixels corresponding to emissions with
488 high energy densities. However, this is only speculation as the PDD triggers that could confirm
489 sustained optical emission had been exhausted by this point in the flash.

490 The second of the single groups in Figure 8 would become important because it marked
491 the initial development of a new branch in the flash that would go on to produce the third +CG
492 stroke at 337 ms. Flash evolution at the time of the third stroke is shown in Figure 9. While this
493 stroke was not accompanied by strong VHF emission (only 5 dB above the baseline RF power
494 during the flash), it was optically bright – producing a LLS group with more than 10% of the
495 energy of the 8-sigma stroke. It likewise has a long VHF tail (12-15 ms following the primary
496 pulse) within which LLS activity could be noted back at the flash origin – again, suggesting that
497 the whole channel was active during this period. The single-event group at 362 ms marks the last
498 time when LLS detected activity near the flash origin until the final phase of the flash.

499 4.3 Channel extension and branching leading up to the fourth +CG stroke

500 The period following the third +CG strokes is marked by continued incremental lateral
501 development of the existing branches along the lightning channel and the later establishment of a
502 new northwestern major branch. The first portion of this period from 450 ms to 550 ms is plotted
503 in Figure 10, and it lacked the sustained VHF emission that we noted previously with the initial
504 development of the flash. The impulsive IC events during this period originated from a broad
505 range of altitudes between 4 km and 7 km. TATR events included isolated IC pulse pairs,
506 sustained featureless emission, and diffuse RF pulses as the northeastern and eastern branches
507 were extended by 1-2 pixel LLS groups illuminating their tips. Small features can also be noted
508 on the order of 1 pixel or less departing from the main channel (light grey features in Figure
509 10c). These smaller features may be short branches or they might be caused by uncertainties in
510 the source locations due to the pixelated LLS grid.

511 The final group during this period established the beginning of a new northern branch
512 that would continue to develop to the northwest over the next few groups and go on to produce
513 the fourth +CG stroke. The initial development of the northwestern branch from 540 ms to 590
514 ms is shown in Figure 11. There are a few RF-only triggers from 540 ms to 550 ms in Figure
515 11e,f followed by sustained RF activity that resembles the initial TATR triggers in the flash.
516 However, the strong RF pulse at the beginning of the sustained RF triggering appears to be a K-
517 change rather than a stroke in this case due to its relatively-slow rise time. This sustained VHF
518 emission lasted ~70 ms and appears to describe leader activity along only the northern branches
519 of the flash (Figure 11c).

520 The time period from 585 ms to 700 ms is shown in Figure 12 and includes the fourth
521 +CG stroke at 593 ms. The VHF pulse reached 12 dB above the RF background and generated
522 the second-most radiant optical group in the LLS flash at 4-sigma. The LLS group had an oblong

523 footprint with the most radiant pixels following the linear path of the northwestern branch
524 (Figure 12c). As with the previous +CG events, a VHF tail can be noted lasting for 20 ms
525 following the stroke. Subsequent groups in Figure 12 describe re-illumination along the
526 northeastern branch of the flash and further extension of some of the smaller branches away from
527 the main channel.

528 4.4 Final development after continuous RF emission ceased

529 The last 480 ms of the flash is shown in the evolution plot in Figure 13. The sustained
530 featureless VHF emission that accompanied the slow leader ceased by 670 ms, and this final
531 period was marked by intermittent impulsive IC events and diffuse K-changes. All but one of the
532 LLS groups occurred along the northeastern branches in the flash. The group at 722 ms is the
533 exception, as it illuminated part of the initial southwestern branch. The group at 752 ms extends
534 the flash to its maximum lateral extent of 82 km across. The final impulsive IC event near 8 km
535 altitude occurred at 820 ms, while the four last impulsive IC events in the flash were located at or
536 below 6 km altitude. The final RF event was a diffuse pulse that had optical coincidence at 1120
537 ms, while the final LLS group was a single-event trigger that occurred 60 ms later along the
538 northernmost extent of the flash structure.

539

540 **5 Conclusion**

541 We use coincident optical and RF instrumentation aboard the FORTE satellite to examine
542 the combined-phenomenology evolution of an oceanic megaflash that was 82 km across and
543 lasted nearly 1.2 s. There are a number of distinct features in the optical / RF signatures that
544 stand out in this flash, which may be unique to this distinct class of lightning.

545 No RF triggers occurred before the first optical event, while the initial RF / optical
546 signals were some of the weakest recorded from the flash. The 591 TATR events produced by
547 this megaflash were dominated by sustained featureless VHF emission that constantly triggered
548 TATR over periods lasting tens to hundreds of milliseconds. Impulsive IC events occurred at
549 altitudes between 3 and 8 km. The LLS groups describe the incremental lateral development of
550 the lightning channel at a typical development speed of $2.6 \times 10^5 \text{ m s}^{-1}$. Three of these groups
551 were particularly radiant and accounted for 5%, 38%, and 17% of the total optical energy from
552 the flash (52% from all three, combined). The top two most radiant groups come from +CG
553 strokes, while the third appears to have resulted from a -CG stroke, though RF waveform
554 analysis was inconclusive. Two additional +CG strokes were also identified whose optical
555 energies did not reach the 1-sigma level for the flash.

556 These observations are consistent with previous ground-based studies that show “spider
557 lightning” in horizontally-propagating flashes occurring as slow negative leaders ($2\text{-}4 \times 10^5 \text{ m s}^{-1}$)
558 that develop at low levels ($\sim 4 \text{ km}$) in mature / dissipating stratiform clouds via the same apparent
559 mechanism as the stepped leaders that precede negative return strokes. Similarities in the general
560 optical / RF phenomenologies and the signatures that are present suggest that we are sensing the
561 same processes from orbit that they recorded at ground level. The sustained RF emission during
562 extensive flash propagation in the optical data confirm that this behavior is related to leader
563 activity in the cloud and provides additional context for our previous assessment of the speed and
564 scale of optical flash development (Peterson et al., 2018).

565

566 **Acknowledgments**

567 Los Alamos National Laboratory is operated by Triad National Security, LLC, under contract
568 number 89233218CNA000001. The data presented in this study are located at Peterson (2020).

569

570 **References**

571 Bitzer, P. M., 2017: Global distribution and properties of continuing current in lightning, *J. Geophys. Res. Atmos.*,
572 **122**, 1033–1041, doi:10.1002/2016JD025532

573 Blakeslee, R. J., H. J. Christian, M.F. Stewart, D.M. Mach, M. Bateman, T.D. Walker, D. Buechler, W.J. Koshak, S.
574 O'Brien, T. Wilson, E.C. Colley, T. Abbott, J. Carter S. Pavelitz, C. Coker, 2014: Lightning Imaging
575 Sensor (LIS) for the International Space Station (ICC): Mission description and science goals, *XV Int. Conf.*
576 *Atmos. Electricity*. Norman, OK, 15pp.

577 Boggs, L. D., N. Liu, M. Peterson, S. Lazarus, M. Splitt, F. Lucena, A. Nag, and H. Rassoul, 2019: First
578 observations of gigantic jets from geostationary orbit. *Geophys. Res. Lett.*, **46**.
579 <https://doi.org/10.1029/2019GL082278>

580 Carey, L. D., M. J. Murphy, T. L. McCormick, and N. W. S. Demetriades, 2005: Lightning location relative to storm
581 structure in a leading-line, trailing-stratiform mesoscale convective system. *J. Geophys. Res.*, **110**, D03105

582 Christian, H. J., R. J. Blakeslee, S. J. Goodman, and D. M. Mach (Eds.), 2000: Algorithm Theoretical Basis
583 Document (ATBD) for the Lightning Imaging Sensor (LIS), NASA/Marshall Space Flight Center,
584 Alabama. (Available as <http://eosps0.gsfc.nasa.gov/atbd/listables.html>, posted 1 Feb. 2000)

585 Christian, H. J., et al., Global frequency and distribution of lightning as observed from space by the Optical
586 Transient Detector, *J. Geophys. Res.*, 108(D1), 4005, doi:[10.1029/2002JD002347](https://doi.org/10.1029/2002JD002347), 2003.

587 Ely, B. L., R. E. Orville, D. C. Lawrence, and C. L. Hodapp, 2008: Evolution of the total lightning structure in a
588 leading-line, trailing-stratiform mesoscale convective system over Houston, Texas. *J. Geophys. Res.*, **113**,
589 doi:10.1029/2007JD008445

590 Goodman, S. J., D. Mach, W. J. Koshak, and R. J. Blakeslee, 2010: GLM Lightning Cluster-Filter Algorithm
591 (LCFA) Algorithm Theoretical Basis Document (ATBD). NOAA NESDIS Center for Satellite

592 Applications and Research. (Available as <https://www.goes->
593 [r.gov/products/ATBDs/baseline/Lightning_v2.0_no_color.pdf](https://www.goes-r.gov/products/ATBDs/baseline/Lightning_v2.0_no_color.pdf), posted 24 Sept. 2010)

594 Goodman, S. J., R. J. Blakeslee, W. J. Koshak, D. Mach, J. Bailey, D. Buechler, L. Carey, C. Schultz, M. Bateman,
595 E. McCaul Jr., and G. Stano, 2013: The GOES-R geostationary lightning mapper (GLM). *J. Atmos. Res.*,
596 **125-126**, 34-49

597 Holden, D. N., C. P. Munson, and J. C. Devenport, 1995: Satellite observations of transionospheric pulse pairs,
598 *Geophys. Res. Lett.*, **22**, 889–892

599 Jacobson, A. R., S. O. Knox, R. Franz, and D. C. Enemark, 1999: FORTE observations of lightning radio-frequency
600 signatures: Capabilities and basic results. *Radio Sci.*, **34** (2), 337– 354, doi:10.1029/1998RS900043

601 Jacobson, A. R., K. L. Cummins, M. Carter, P. Klingner, D. Roussel-Dupré, and S. O. Knox, 2000: FORTE radio-
602 frequency observations of lightning strokes detected by the National Lightning Detection Network. *J.*
603 *Geophys. Res.*, **105** (D12), 15653– 15662, doi:10.1029/2000JD900103

604 Koshak, W. J., R. J. Solakiewicz, D. D. Phanord, and R. J. Blakeslee, 1994: Diffusion model for lightning radiative
605 transfer. *J. Geophys. Res.*, **99**(D7), 14361– 14371, doi:10.1029/94JD00022

606 Koshak, W. J., 2010: Optical characteristics of OTD flashes and the implications for flash-type discrimination. *J.*
607 *Atmos. Oceanic. Technol.*, **27**, 1,822 – 1,838

608 Lang, T. J., S. A. Rutledge, and K. C. Wiens, 2004: Origins of positive cloud-to-ground lightning in the stratiform
609 region of a mesoscale convective system. *Geophys. Res. Lett.*, **31**, doi: 10.1029/2004GL019823

610 Lang, T., S. Pédeboy, W. Rison, R. Cerveny, J. Montanyà, S. Chauzy, D. MacGorman, R. Holle, E. Ávila, Y.
611 Zhang, G. Carbin, E. Mansell, Y. Kuleshov, T. Peterson, M. Brunet, F. Driouech, and D. Krahenbuhl,
612 2017: WMO World Record Lightning Extremes: Longest Reported Flash Distance and Longest Reported
613 Flash Duration. *Bull. Amer. Meteor. Soc.* **98**, 1153–1168, <https://doi.org/10.1175/BAMS-D-16-0061.1>

614 Lang, T., and S. A. Rutledge, 2008: Kinematic, microphysical, and electrical aspects of an asymmetric bow echo
615 mesoscale convective system observed during STEPS. *J. Geophys. Res.*, **113**, doi: 10.1029/2006JD007709

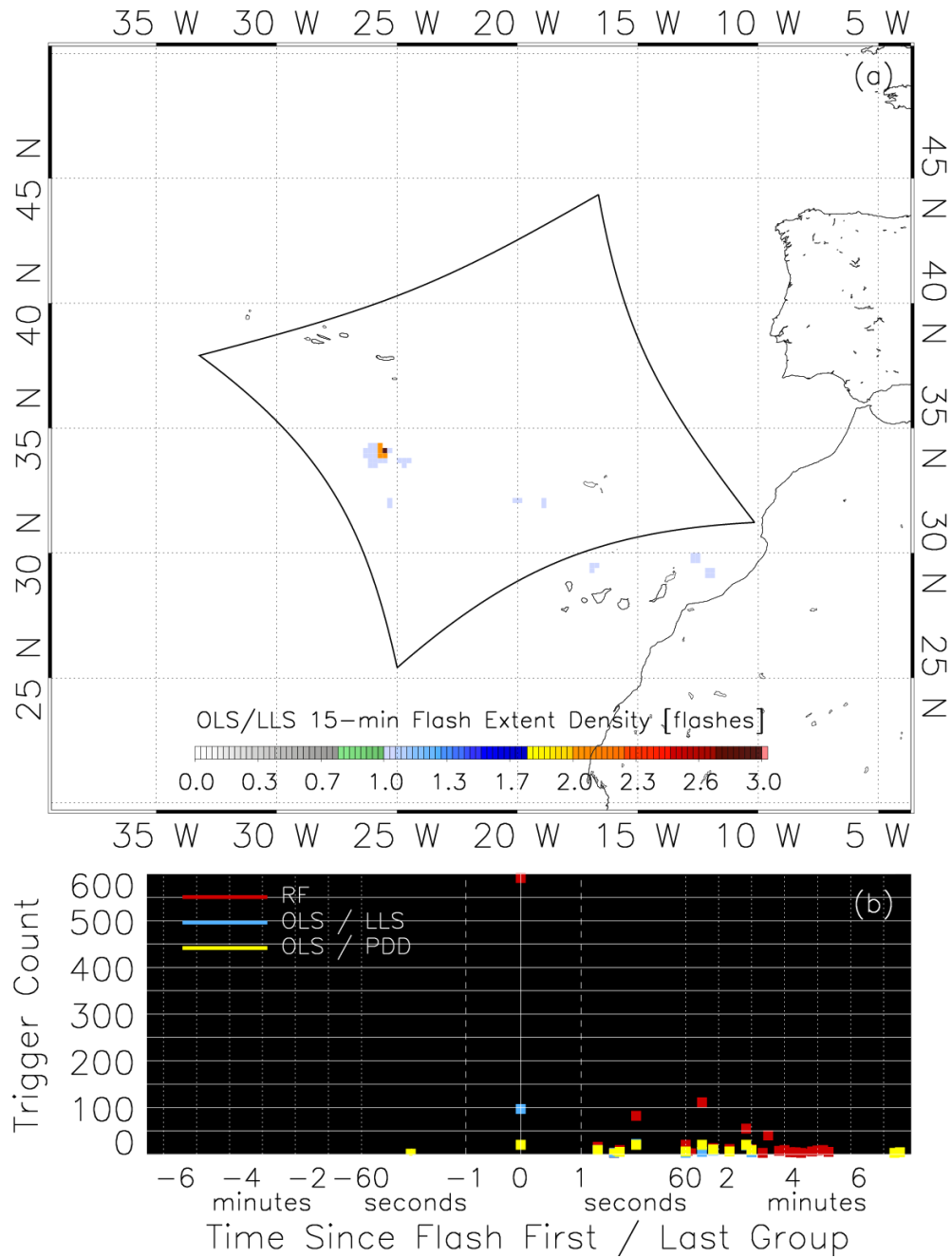
616 Light, T. E., D. M. Suszcynsky, M. W. Kirkland, and A. R. Jacobson, 2001a: Simulations of lightning optical
617 waveforms as seen through clouds by satellites. *J. Geophys. Res.*, **106**, D15, 17103–17114, doi:
618 10.1029/2001JD900051

- 619 Light, T. E., D. M. Suszcynsky, and A. R. Jacobson, 2001b: Coincident radio frequency and optical emissions from
620 lightning, observed with the FORTE satellite. *J. Geophys. Res.*, 106(D22), 28223– 28231,
621 doi:10.1029/2001JD000727
- 622 Lojou, J.-Y., K. L. Cummins, 2004: On the representation of two- and three-dimensional total lightning information.
623 In Preprints, Conference on Meteorological Applications of Lightning Data (pp. Paper 2.4, AMS Annual
624 Meeting, San Diego, CA, USA)
- 625 Marshall, T. C., and W. D. Rust, 1993: Two types of vertical electrical structures in stratiform precipitation regions
626 of mesoscale convective systems. *Bull. Amer. Meteor. Soc.*, **74**, 2159-2170
- 627 Marshall, T. C., M. Stolzenburg, P. R. Krehbiel, N. R. Lund, and C. R. Maggio, 2009. Electrical evolution during
628 the decay stage of New Mexico thunderstorms, *J. Geophys. Res.*, **114**, D02209, doi:
629 10.1029/2008JD010637
- 630 Mazur, V., X.-M. Shao, and P. R. Krehbiel, 1998: “Spider” lightning in intracloud and positive cloud-to-ground
631 flashes. *J. Geophys. Res.*, **103** (D16), 19811– 19822, doi:10.1029/98JD02003
- 632 Peterson, M., 2020, CIERRA-FORTE Flash Cluster Data, <https://doi.org/10.7910/DVN/63FWWU>, Harvard
633 Dataverse, DRAFT VERSION
- 634 Peterson, M. J. and C. Liu, 2011: Global statistics of lightning in anvil and stratiform regions over the tropics and
635 subtropics observed by TRMM, *J. Geophys. Res.*, **116**, D23, doi: 10.1029/2011JD015908
- 636 Peterson, M. J. and C. Liu, 2013: Characteristics of lightning flashes with exceptional illuminated areas, durations,
637 and optical powers and surrounding storm properties in the tropics and inner subtropics, *J. Geophys. Res.*,
638 **118**, 11,727-11,740, doi: 10.1002/jgrd.50715
- 639 Peterson, M. J., W. Deierling, C. Liu, D. Mach, C. Kalb, 2017a: The properties of optical lightning flashes and the
640 clouds they illuminate. *J. Geophys. Res. Atmos.*, **122**, 423–442, doi:10.1002/2016JD025312
- 641 Peterson, M. J., S. Rudlosky, and W. Deierling, 2017b: The evolution and structure of extreme optical lightning
642 flashes. *J. Geophys. Res. Atmos.*, **122**, doi: 10.1002/2017JD026855
- 643 Peterson, M., S. Rudlosky, and W. Deierling, 2018: Mapping the Lateral Development of Lightning Flashes from
644 Orbit. *J. Geophys. Res. Atmos.*, **123**, 9674– 9687. <https://doi.org/10.1029/2018JD028583>
- 645 Peterson, M., S. Rudlosky, 2019: The time evolution of optical lightning flashes. *J. Geophys. Res.*, **124**, 333– 349.
646 <https://doi.org/10.1029/2018JD028741>

- 647 Peterson, M., T. E. L. Light, and X.-M. Shao, 2020a: Combined Optical and Radio-Frequency Perspectives on
648 Hybrid Cloud-to-Ground Lightning Observed by the FORTE Satellite, this issue (submitted as companion
649 paper)
- 650 Prueitt, M. L., 1963: The excitation temperature of lightning. *J. Geophys. Res.*, **68** (3), 803– 811,
651 doi:10.1029/JZ068i003p00803
- 652 Rison, W., R.J. Thomas, P.R. Krehbiel, T. Hamlin, and J. Harlin, 1999: A GPS-based three-dimensional lightning
653 mapping system: initial observations in central New Mexico. *Geophys. Res. Lett.*, **26**, 23, 3573-3576
- 654 Rutledge, S. A., and D. R. MacGorman, 1988: Cloud-to-ground lightning activity in the 10-11 June 1985 mesoscale
655 convective system observed during the Oklahoma-Kansas PRESTORM project. *Mon. Wea. Rev.*, **116**,
656 1393–1408
- 657 SSEC, 2019: Satellite Data Services Inventory. Accessed 7 May 2019, <https://qcweb.ssec.wisc.edu/inventory/>
- 658 Stolzenburg, M., T.C. Marshall, W. D. Rust, and B.F. Smull, 1994: Horizontal distribution of electrical and
659 meteorological conditions across the stratiform region of a mesoscale convective system. *Mon. Wea. Rev.*,
660 **122**, 1777–1797
- 661 Suszcynsky, D. M., M. W. Kirkland, A. R., Jacobson, R. C. Franz, S. O. Knox, J. L. L. Guillen, and J. L. Green,
662 2000: FORTE observations of simultaneous VHF and optical emissions from lightning: Basic
663 phenomenology. *J. Geophys. Res.*, **105** (D2), 2191– 2201, doi:10.1029/1999JD900993
- 664 Suszcynsky, D. M., T. E. Light, S., Davis, J. L., Green, J. L. L. Guillen, and W. Myre, 2001: Coordinated
665 observations of optical lightning from space using the FORTE photodiode detector and CCD imager. *J.*
666 *Geophys. Res.*, **106** (D16), 17897– 17906, doi:10.1029/2001JD900199
- 667 Thomas, R., P.R. Krehbiel, W. Rison, T. Hamlin, D. J. Boccippio, S. J. Goodman, and H. J. Christian, 2000:
668 Comparison of ground-based 3-dimensional lightning mapping observations with satellite-based LIS
669 observations in Oklahoma. *Geophys. Res. Lett.*, **27**, 12, 1,703-1,706.
- 670 Thomson, L.W. and E.P. Krider, 1982: The Effects of Clouds on the Light Produced by Lightning. *J. Atmos. Sci.*,
671 **39**, 2051–2065, [https://doi.org/10.1175/1520-0469\(1982\)039<2051:TEOCOT>2.0.CO;2](https://doi.org/10.1175/1520-0469(1982)039<2051:TEOCOT>2.0.CO;2)
- 672 Tillier, C. E., S. F. Edgington, H. J. Christian, and P. M. Bitzer, 2019: The First Stereo Views of Lightning from
673 Space: Double the GLMs, Double the Fun. *99th American Meteorological Society Annual Meeting*,

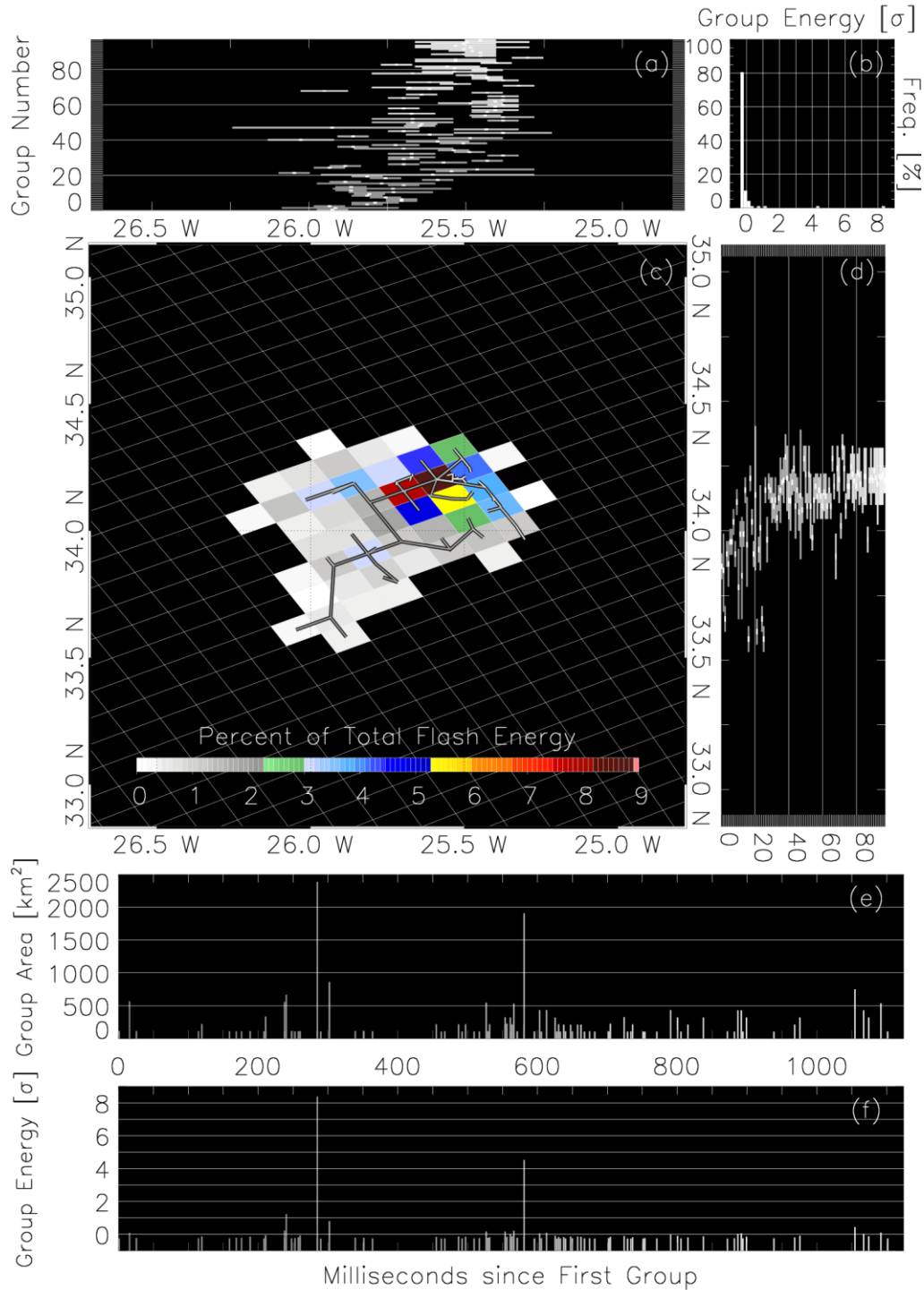
674 Phoenix, AZ, Amer. Meteor. Soc., TJ11.1,
675 <https://ams.confex.com/ams/2019Annual/webprogram/Paper350902.html>
676 Winn, W. P., G. D. Aulich, S. J. Hunyady, K. B. Eack, H. E. Edens, P. R. Krehbiel, W. Rison, and R. G.
677 Sonnenfeld, 2011: Lightning leader stepping, K changes, and other observations near an intracloud flash. *J.*
678 *Geophys. Res.*, **116**, D23115, doi:10.1029/2011JD015998
679
680

681

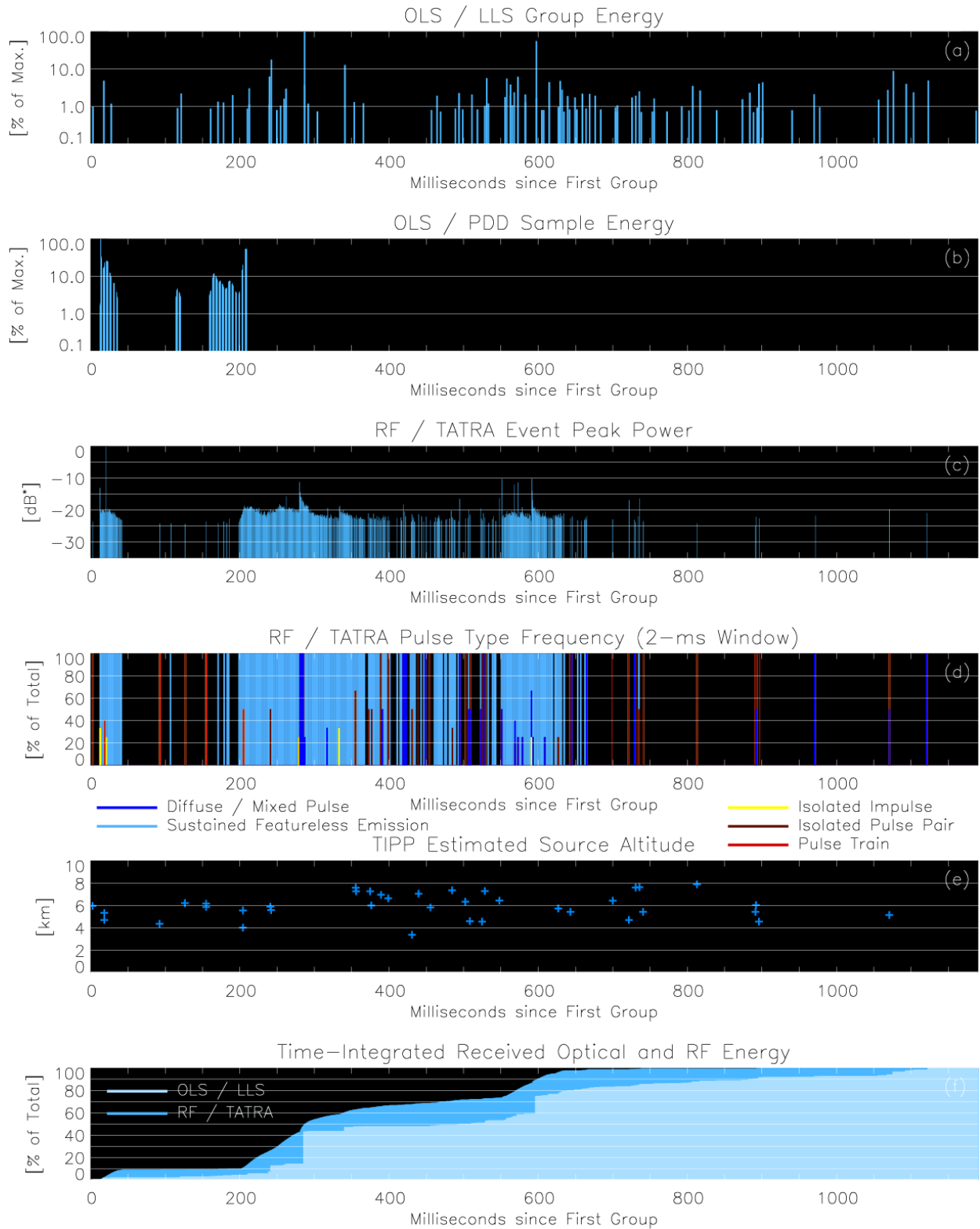


682
683
684
685
686
687

Figure 1. FORTE LLS lightning activity near the flash of interest. (a) FED across the LLS FOV and (b) optical and RF trigger rates during the 15-minute window surrounding the flash. Because lightning was infrequent across the FORTE FOV during the flash window, triggers from other flashes are unlikely.

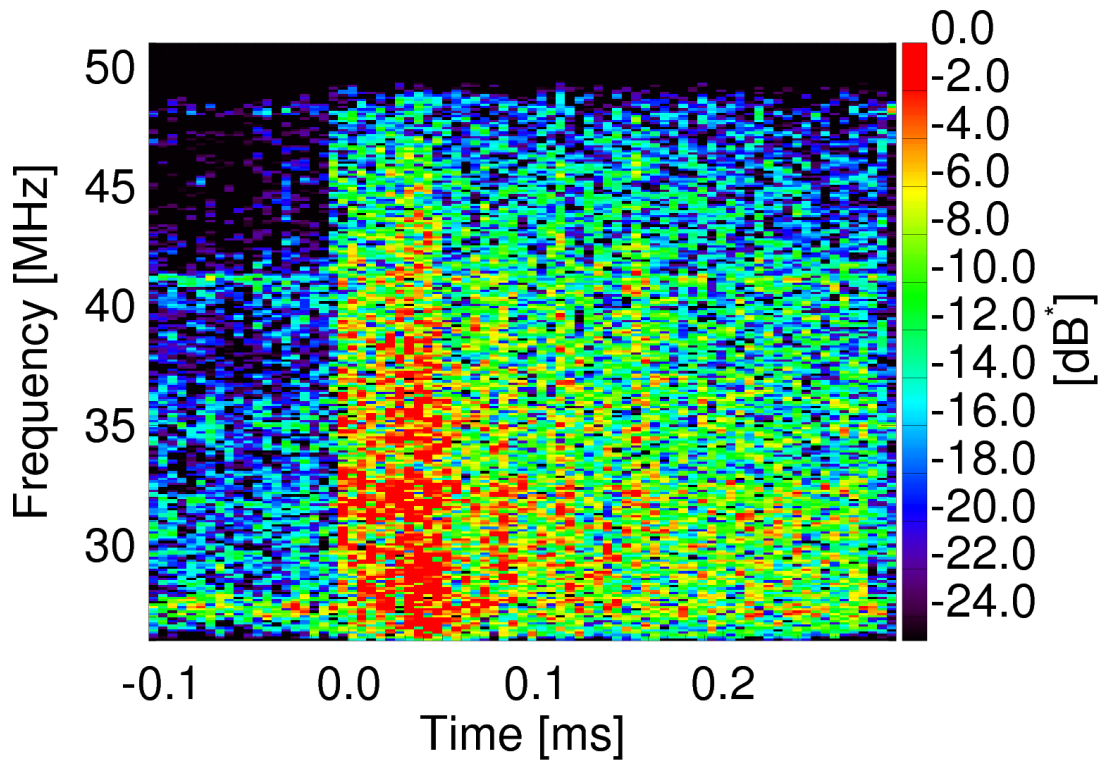


688
 689 **Figure 2.** Evolution plot for the LLS flash. (a) group extent by longitude, (b) group energy distribution, (c) plan
 690 view of flash energy (color contour) and group extent (line segments), (d) group extent by latitude, (e) timeseries of
 691 group area, and (f) timeseries of group energy. Group energies are expressed as a sigma level relative to the average
 692 group energy in the flash. The greyscale in all plots represents the group number.
 693



694
695
696
697
698
699

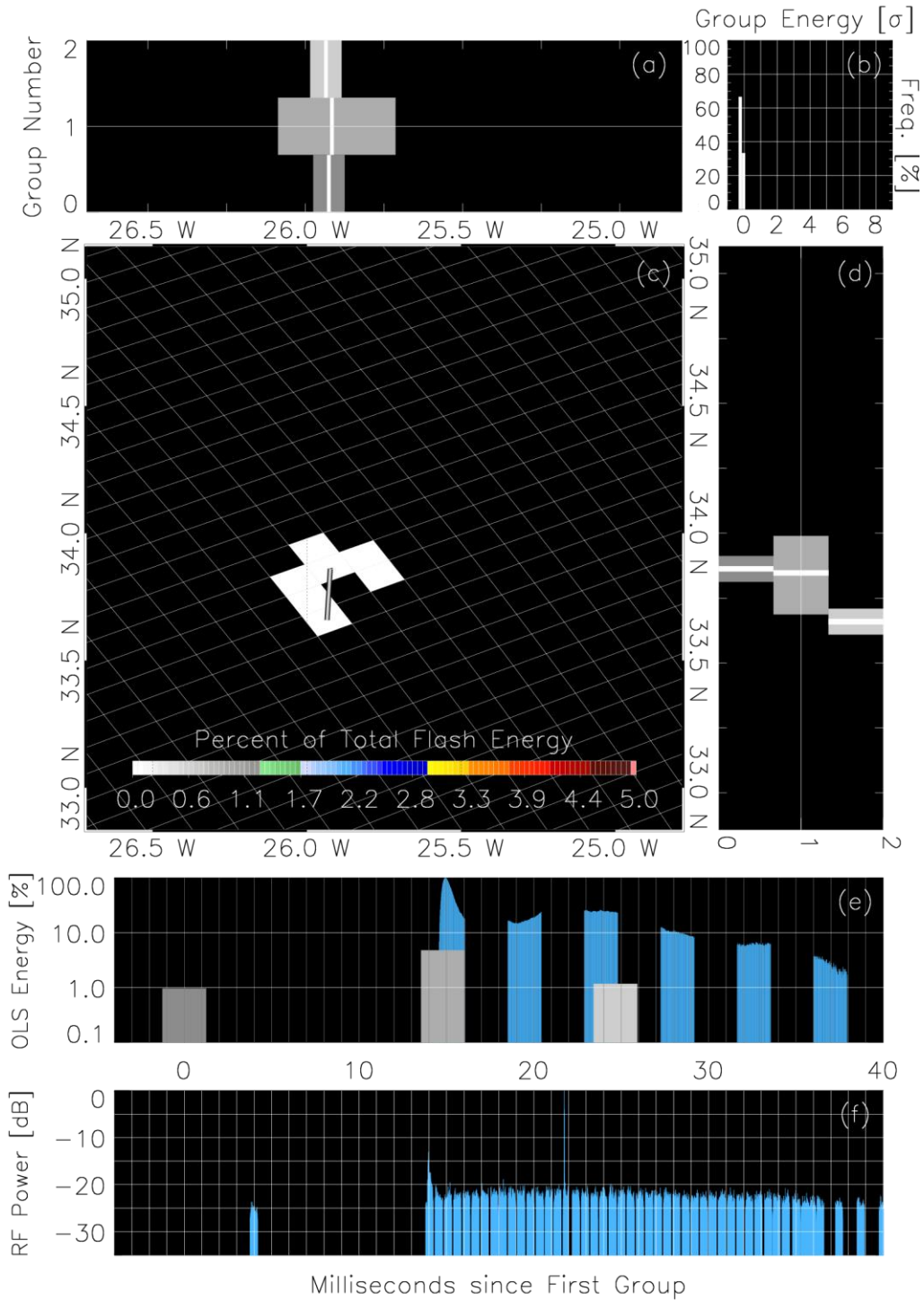
Figure 3. Timeseries showing the combined optical / RF evolution of the flash. (a) LLS and (b) optical energies. (c) TATR event peak RF power. (d) TATR pulse classification shown as the frequency of each pulse type in a 2-ms window. (e) estimated altitude of in-cloud (TIPP) sources. (f) time-integrated optical and RF energies over the flash duration



700
701
702
703
704

Figure 4. Spectrogram showing normalized RF power over the lowband frequency range as a function of time sensed by TATR during the first +CG event at 14 ms into the LLS flash. The sharp onset and long-duration pulse are common VHF features associated with +CGs.

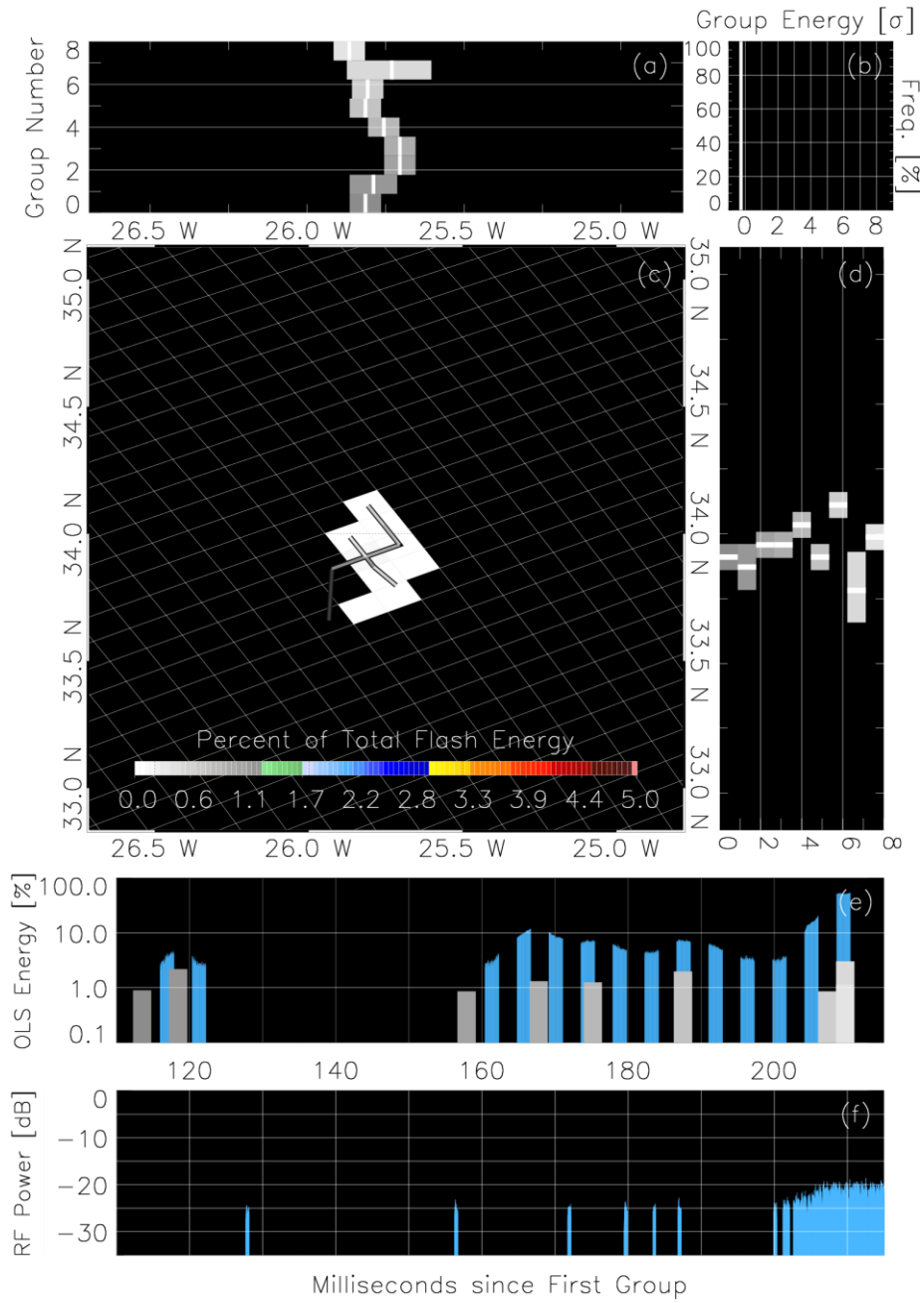
705
706



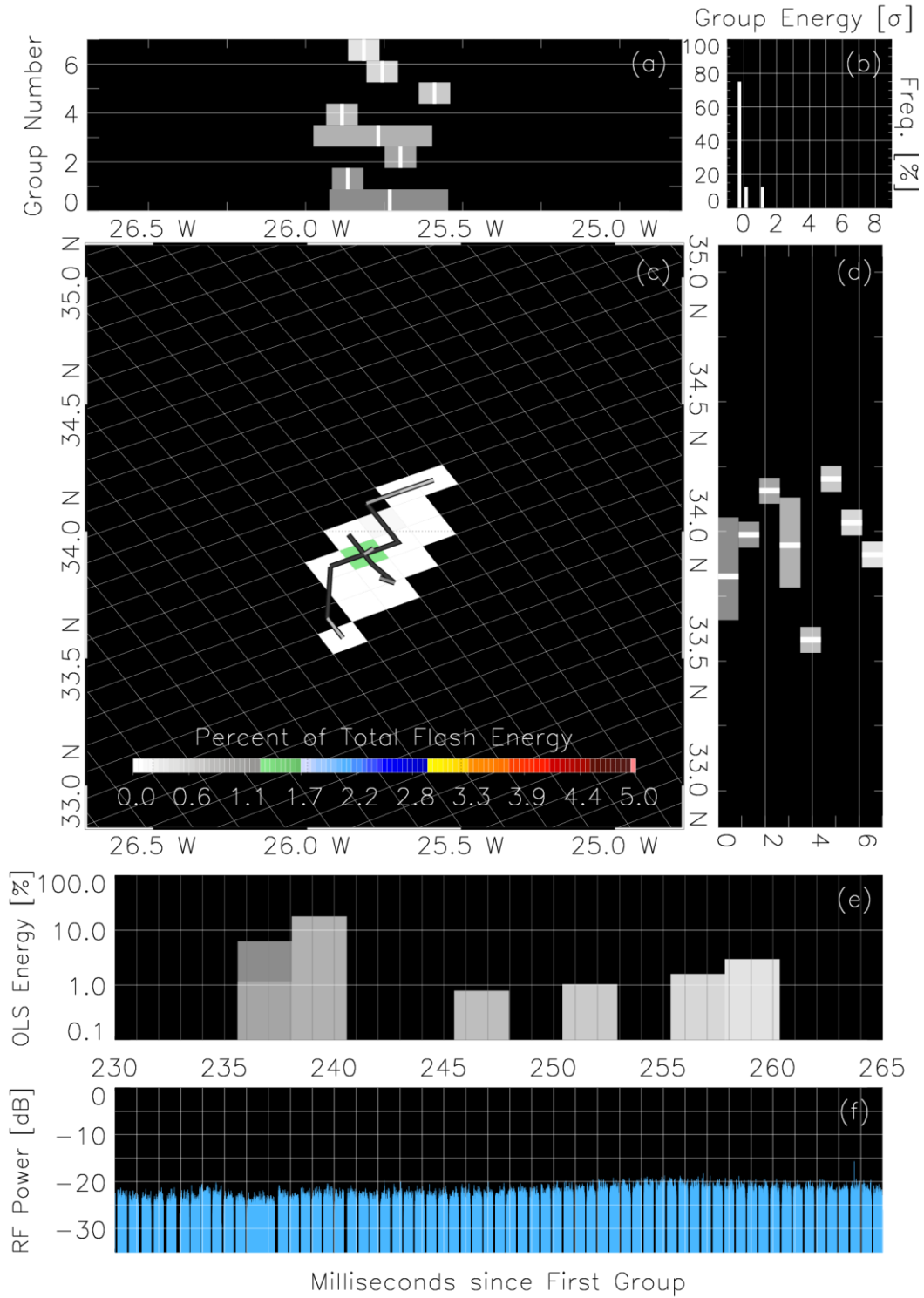
707
708
709
710
711

Figure 5. Evolution plot for the first 40 ms of optical triggers in the flash. Identical to Figure 3, but with LLS group area replaced by TATR RF power (f) and PDD data plotted blue in (e)

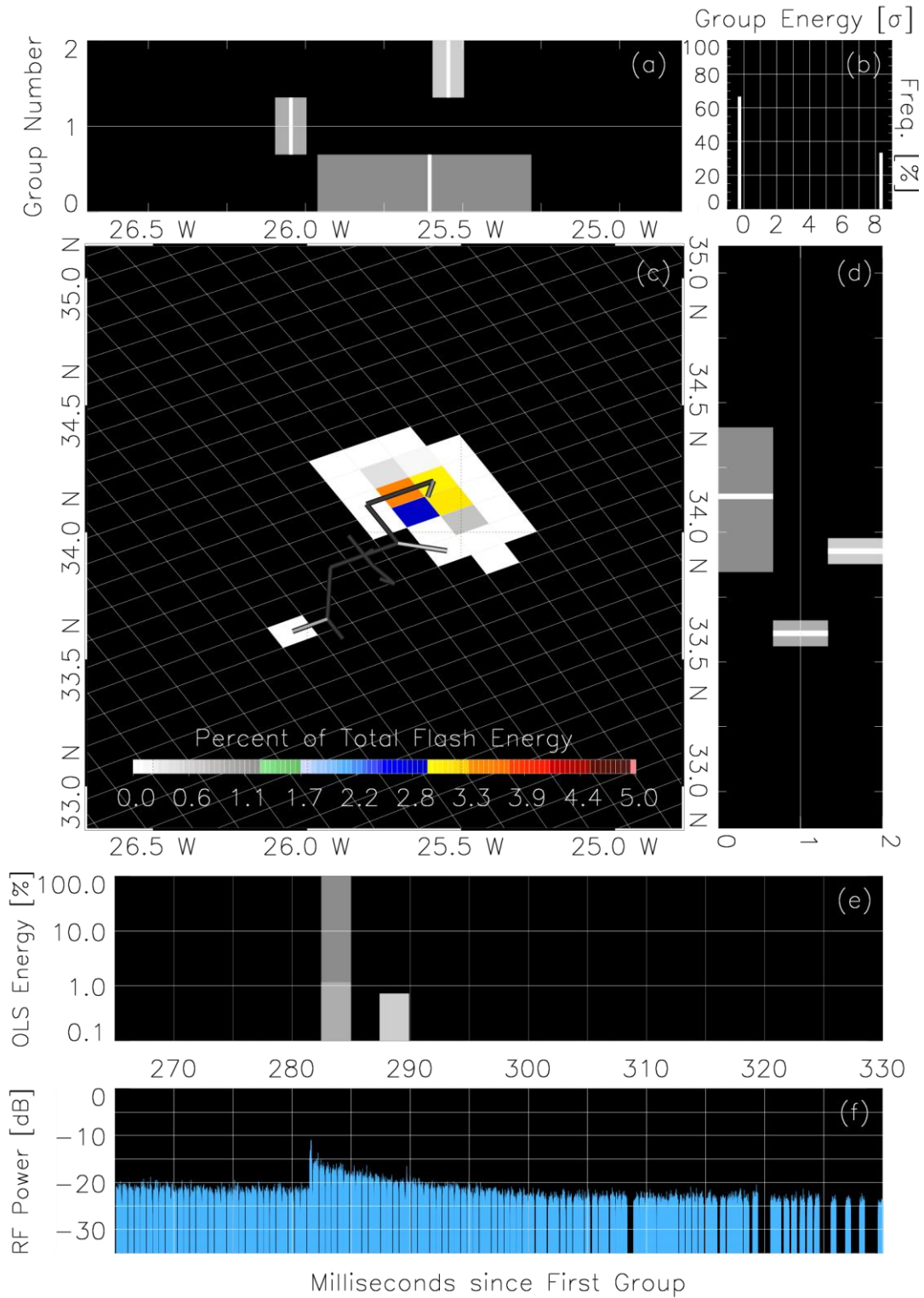
712



713 **Figure 6.** Same as Figure 5, but for the period 110 ms – 215 ms that begins the longest period of sustained PDD /
 714 TATR triggering
 715
 716

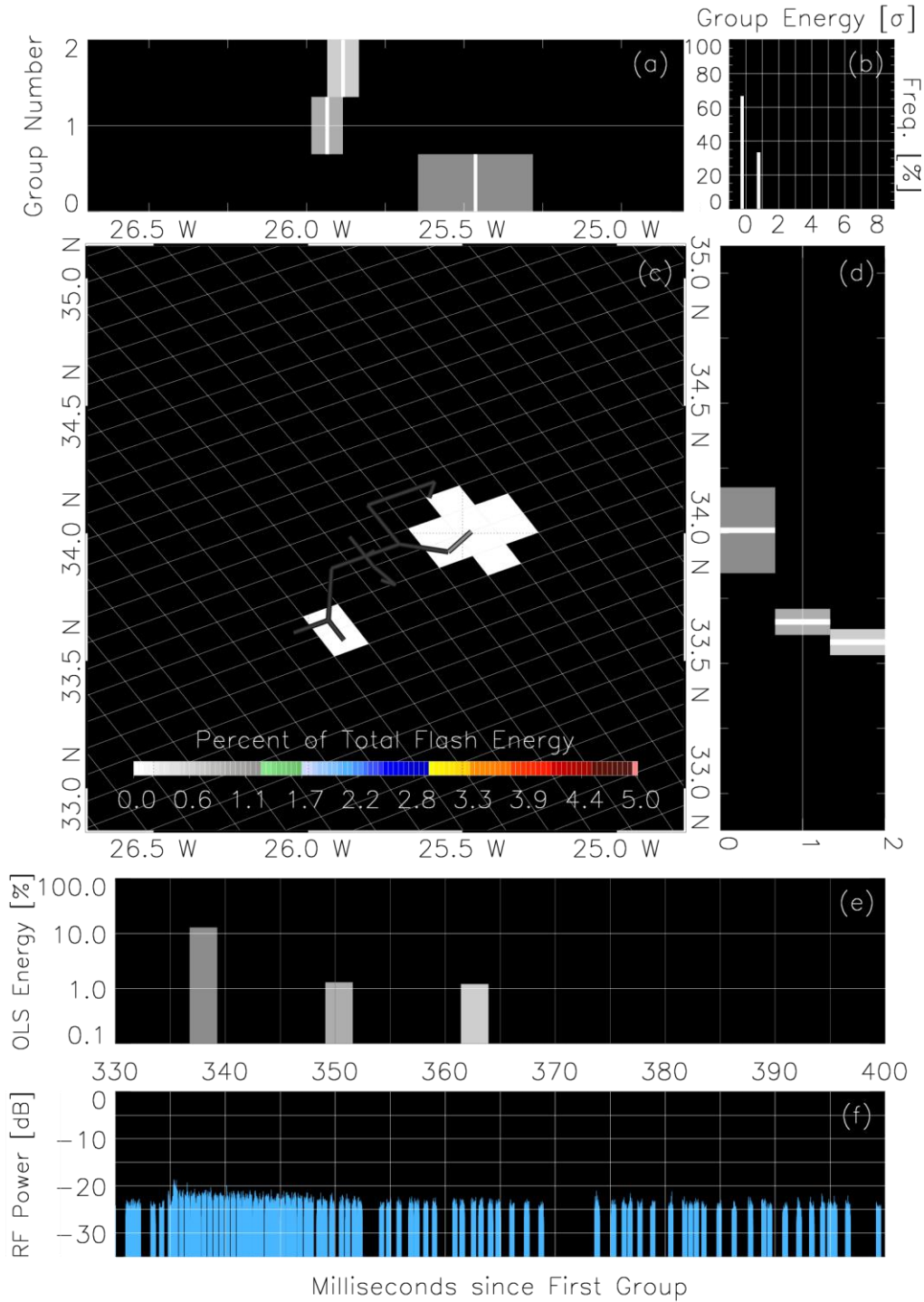


717
 718 **Figure 7.** Same as Figure 5, but for the period 230 ms – 265 ms during the initial development phase of the spider
 719 flash
 720



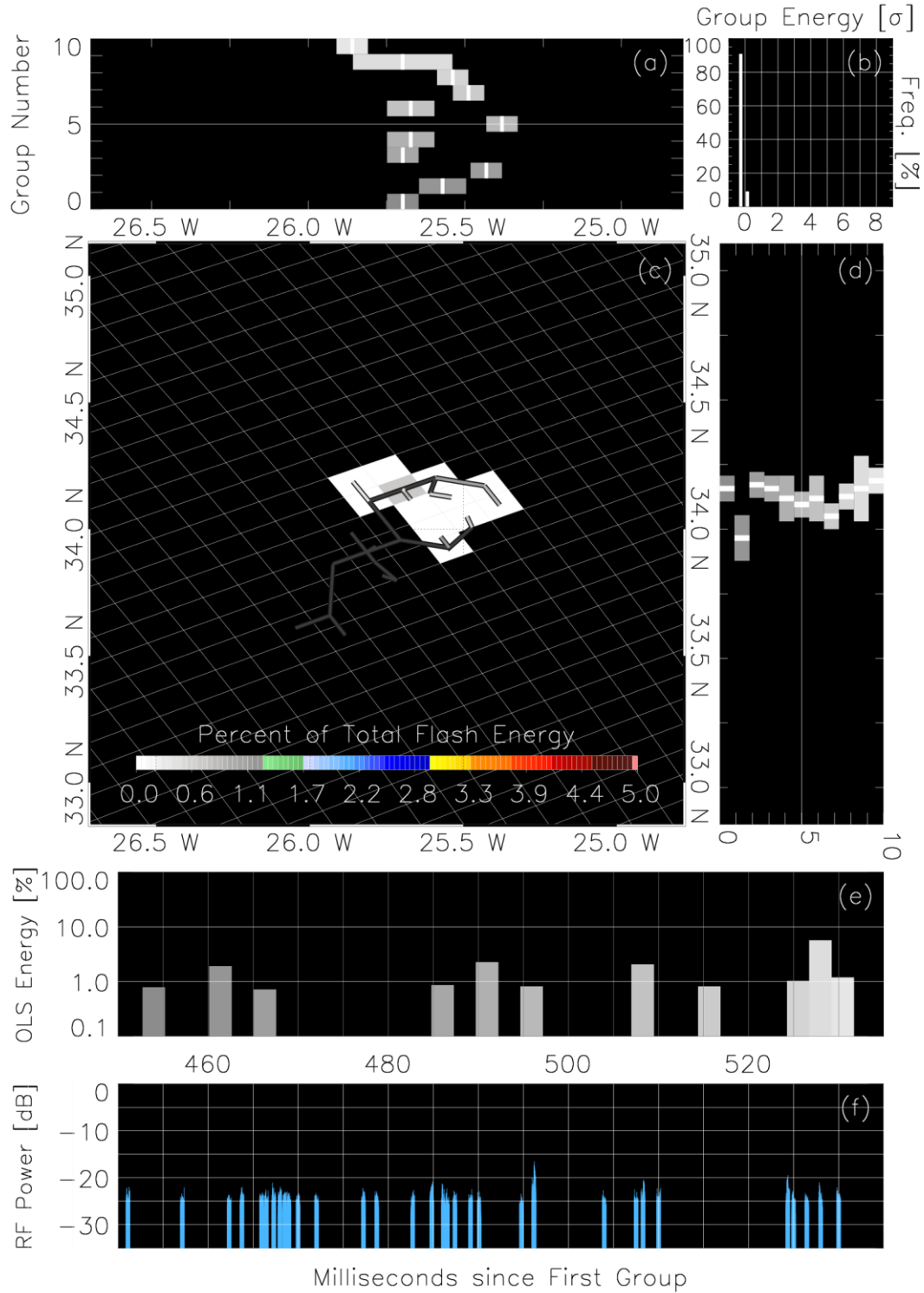
721
722
723
724

Figure 8. Same as Figure 5, but for the period 265 ms – 330 ms that includes the first possible +CG stroke

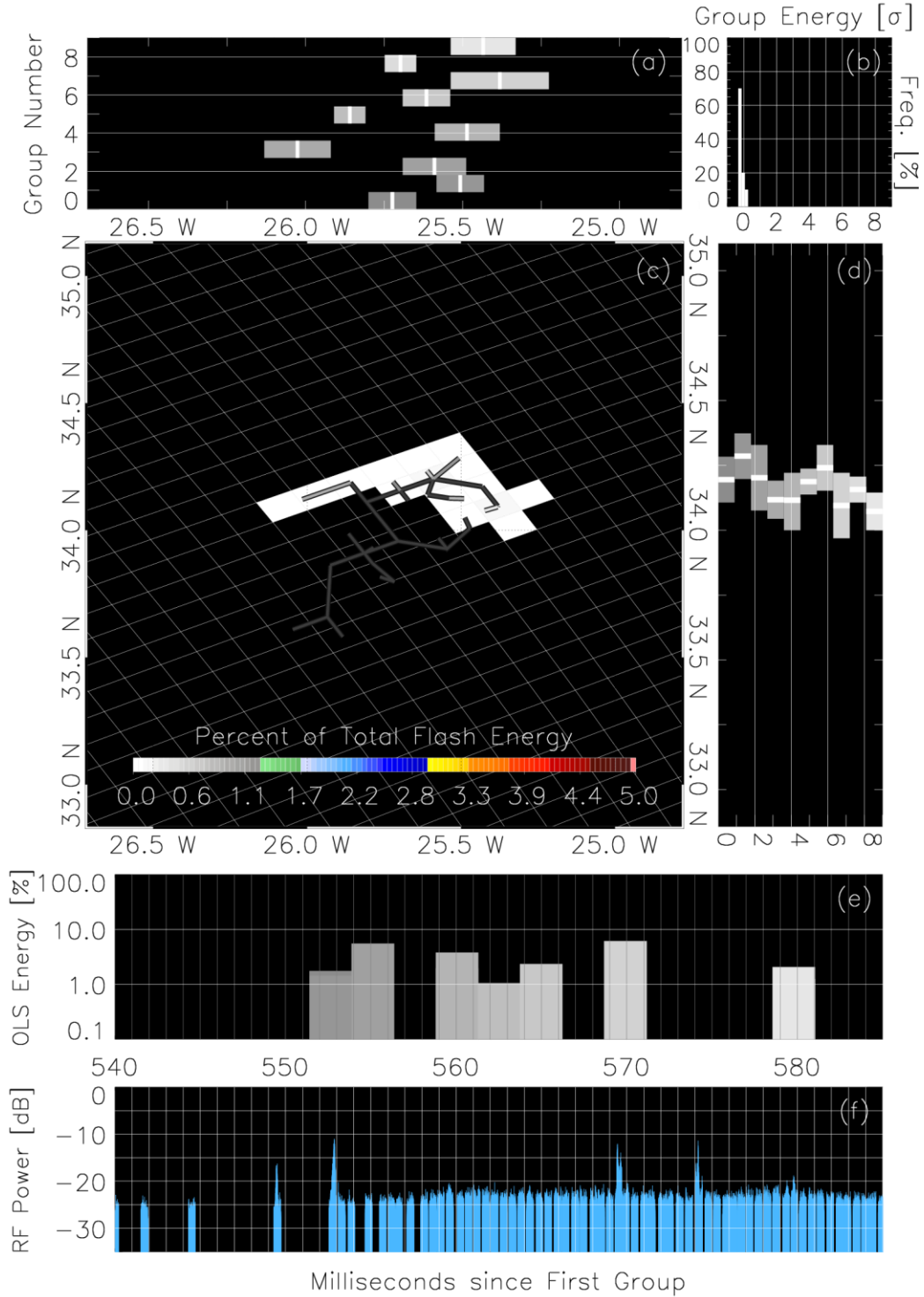


725
726
727
728

Figure 9. Same as Figure 5, but for the period 330 ms – 400 ms that shows a possible (questionable) second +CG stroke in a different location than Figure 8

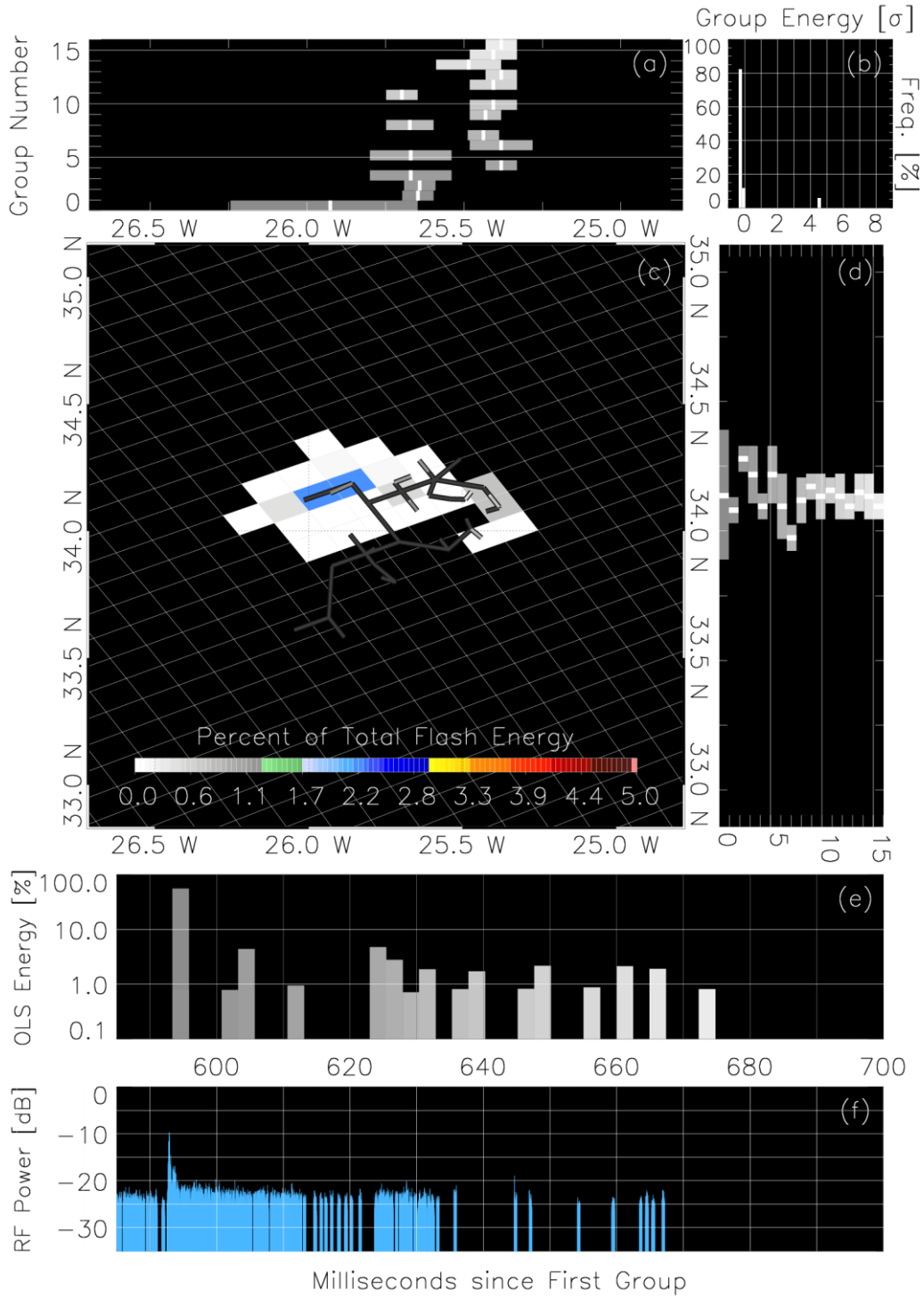


729
 730 **Figure 10.** Same as Figure 5, but for the period 450 ms – 535 ms showing additional lateral development ending
 731 with the start of a new main branch to the northwest
 732

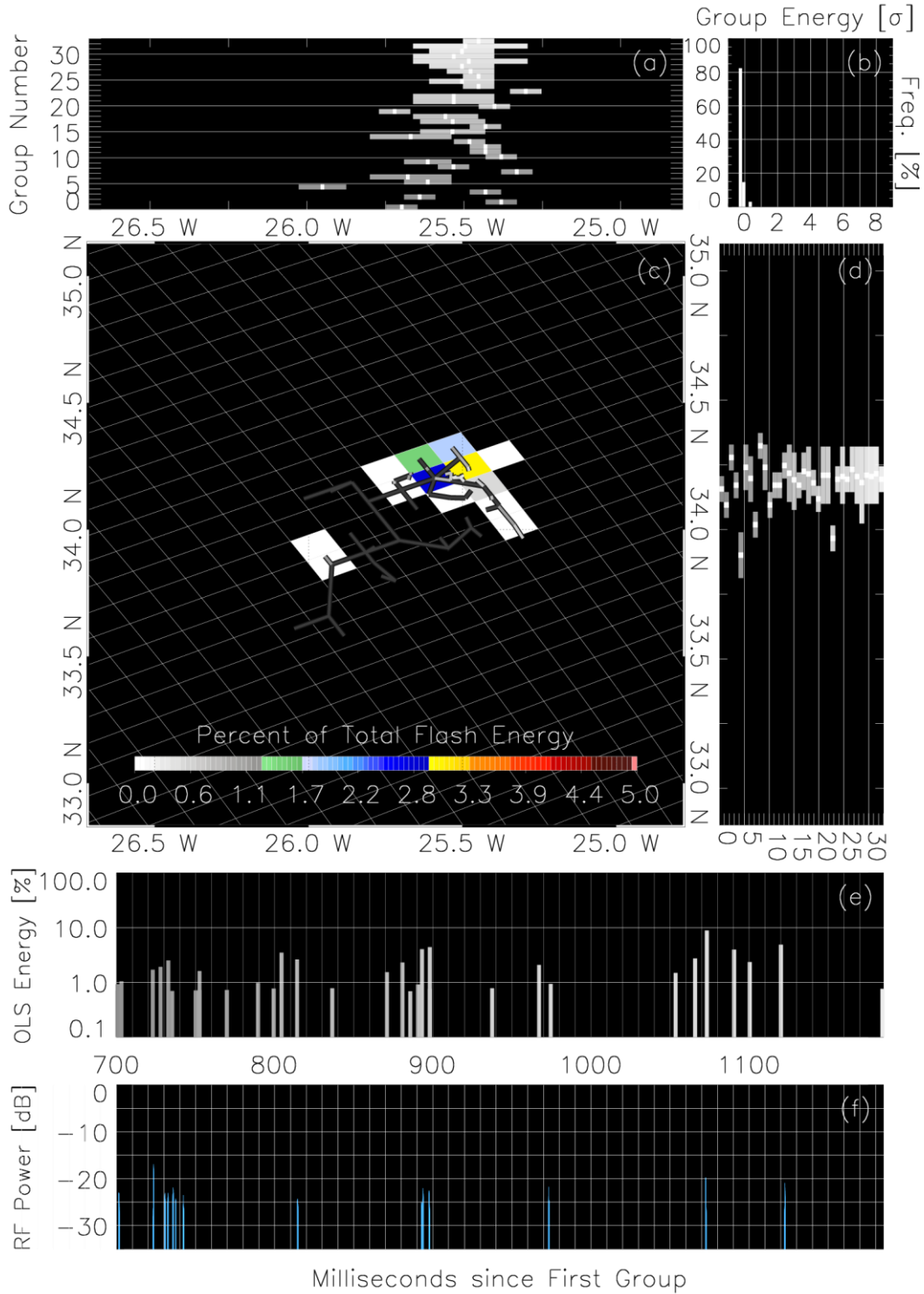


733
734
735
736

Figure 11. Same as Figure 5, but for the period 540 ms – 585 ms where sustained TATR triggering resumes after a diffuse VHF pulse



737
 738 **Figure 12.** Same as Figure 5, but for the period 585 ms – 700 ms showing a possible (questionable) third +CG
 739 stroke along the new northwest branch
 740



741
 742 **Figure 13.** Same as Figure 5, but for the period 700 ms – 1180 ms that documents the final LLS / TATR pulses after
 743 the sustained VHF emission has ceased
 744

Figure 1.

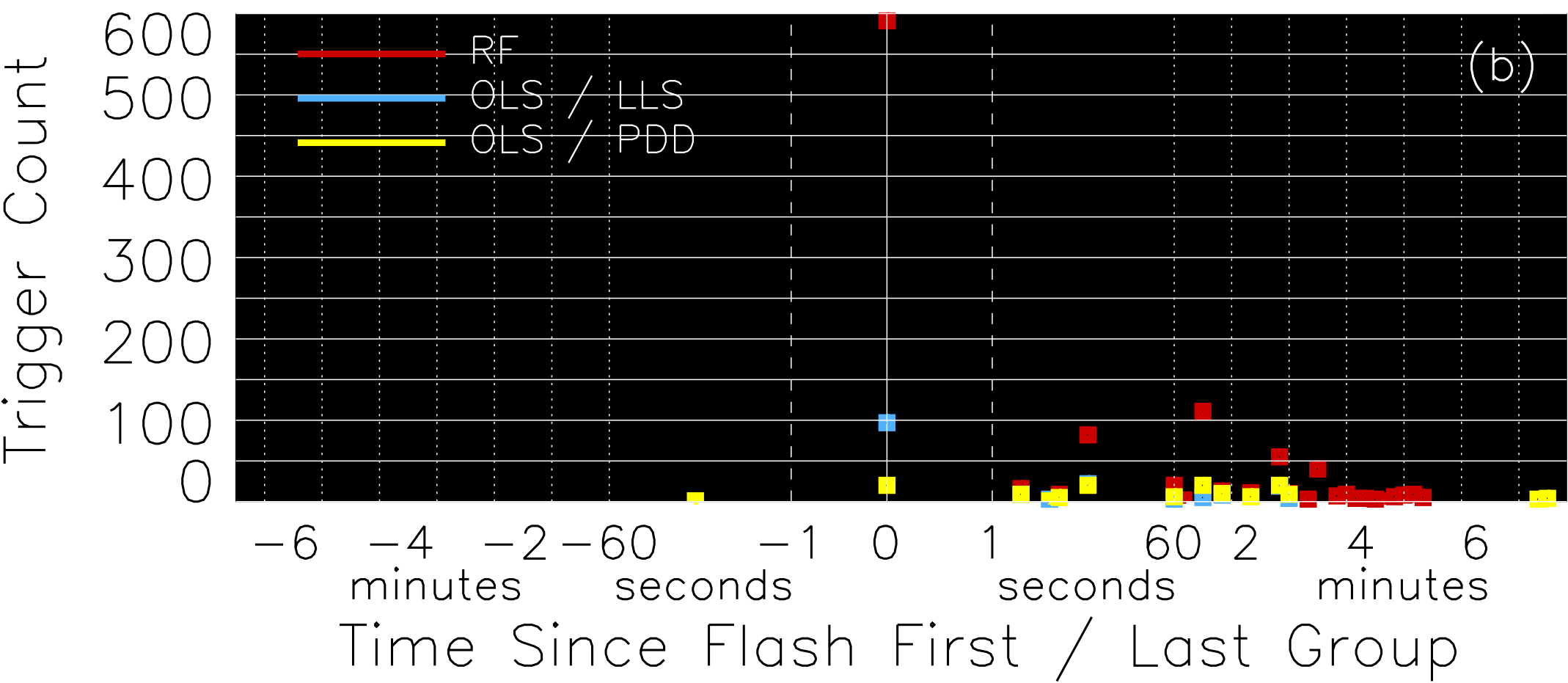
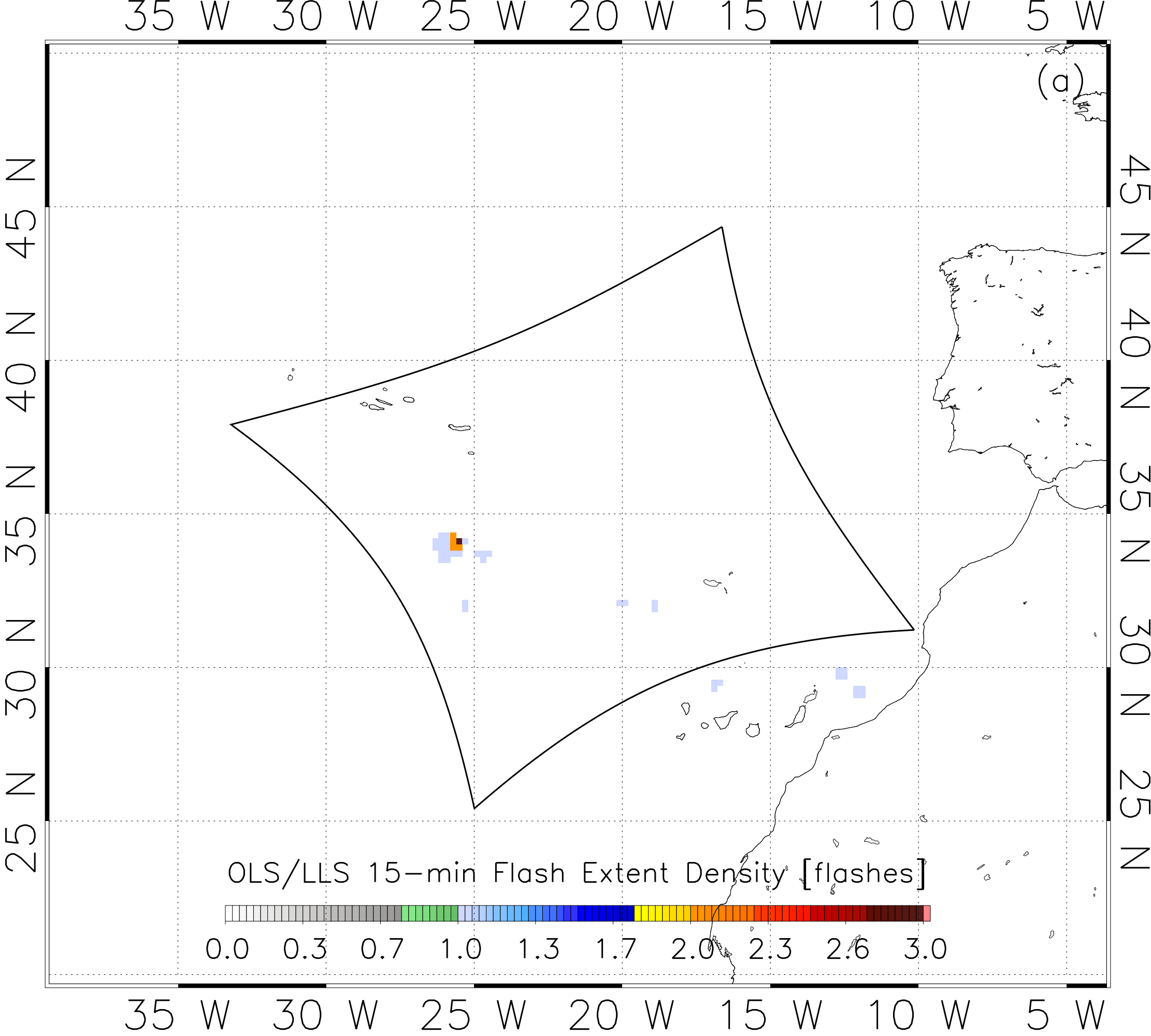


Figure 2.

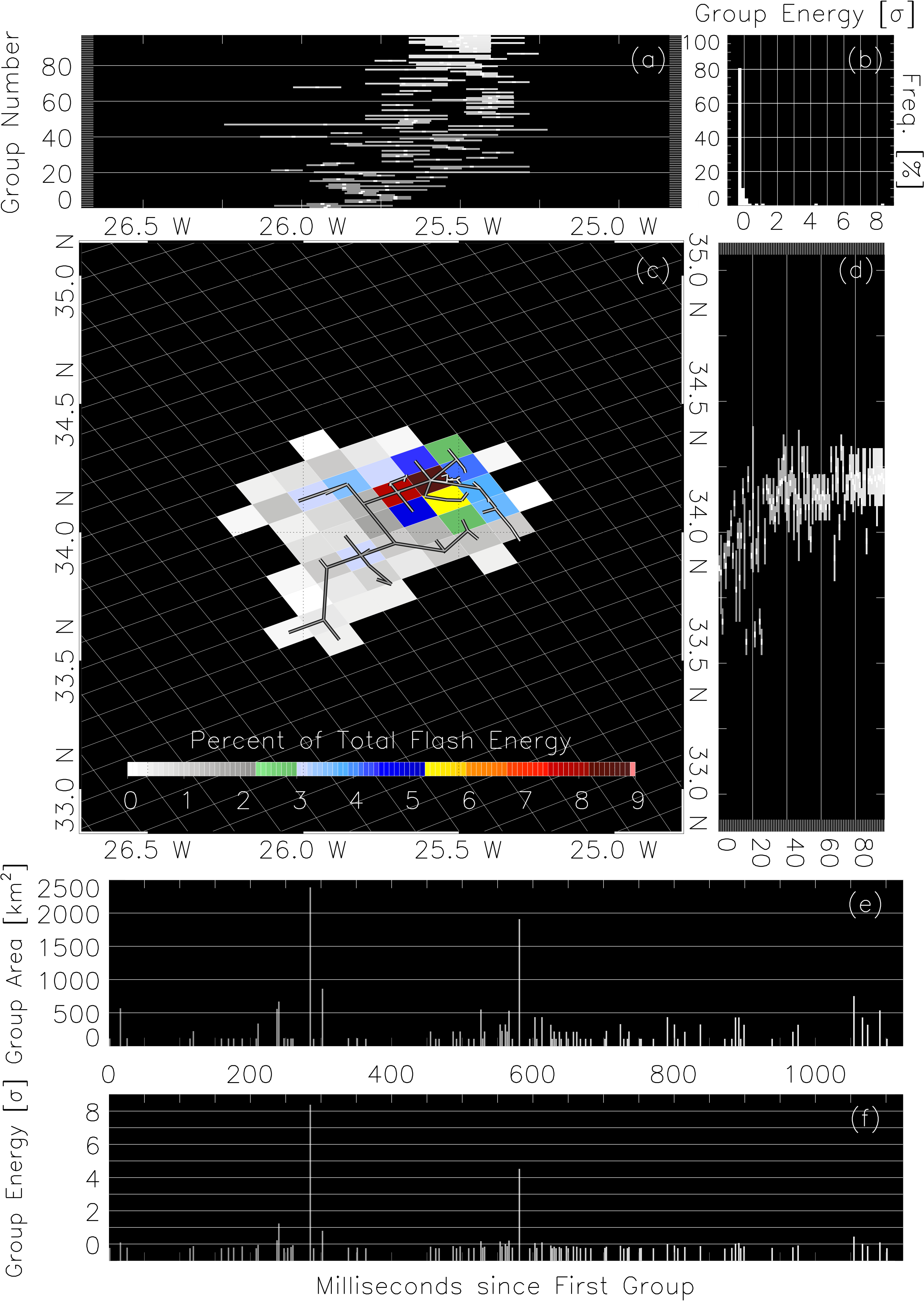


Figure 3.

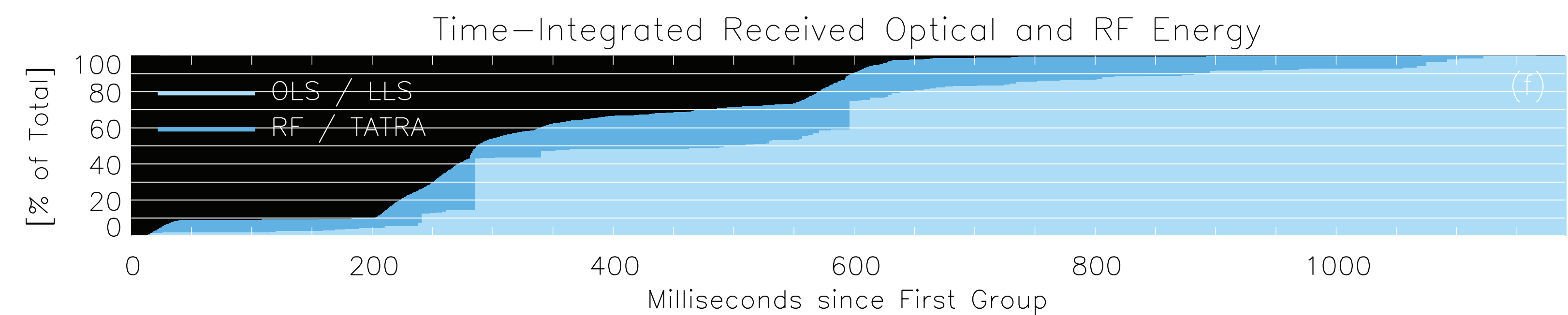
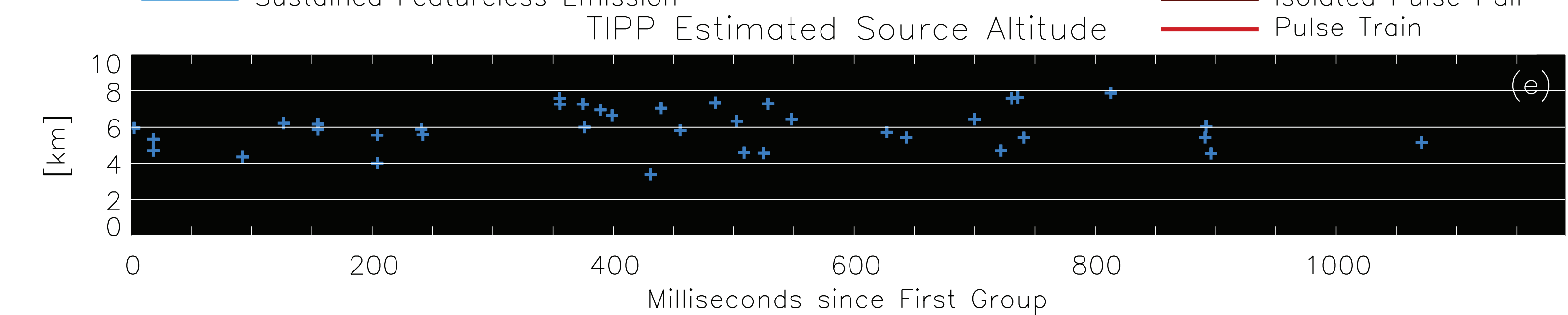
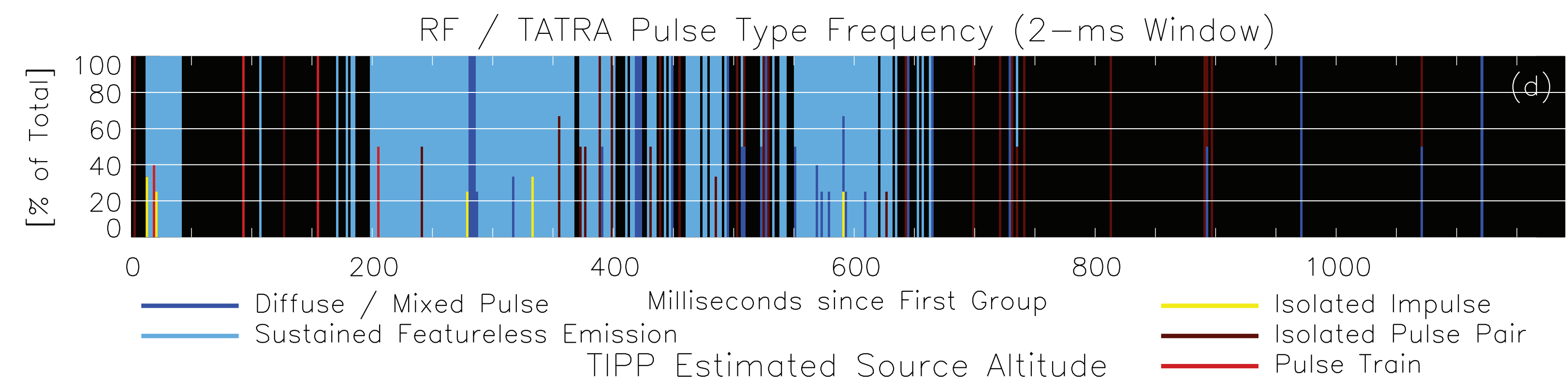
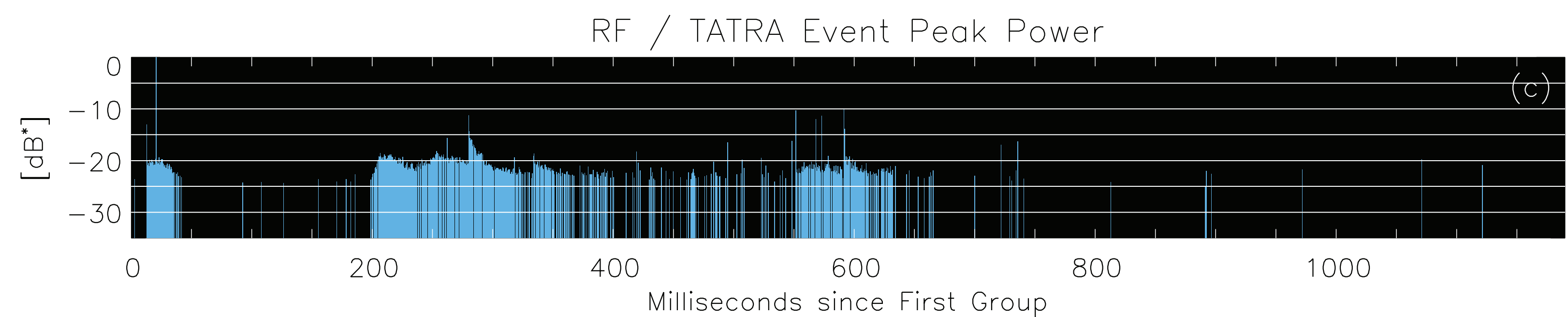
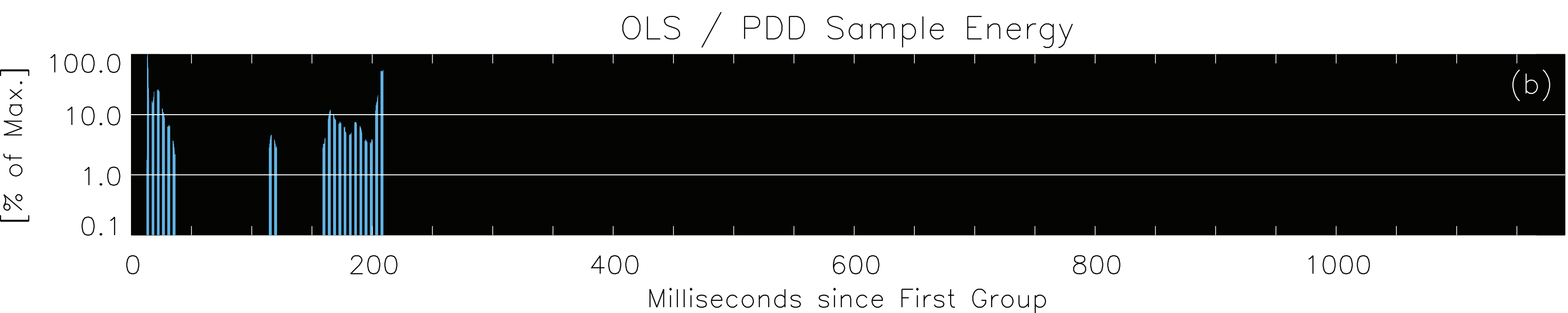
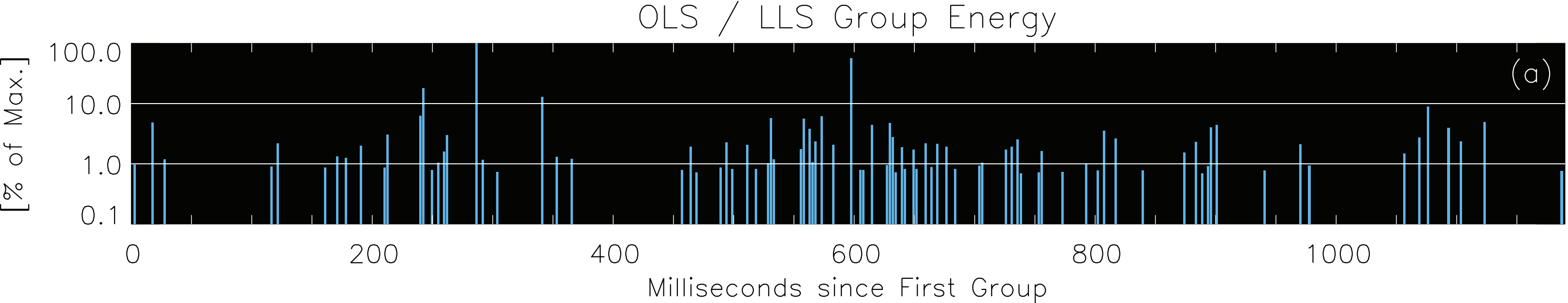


Figure 4.

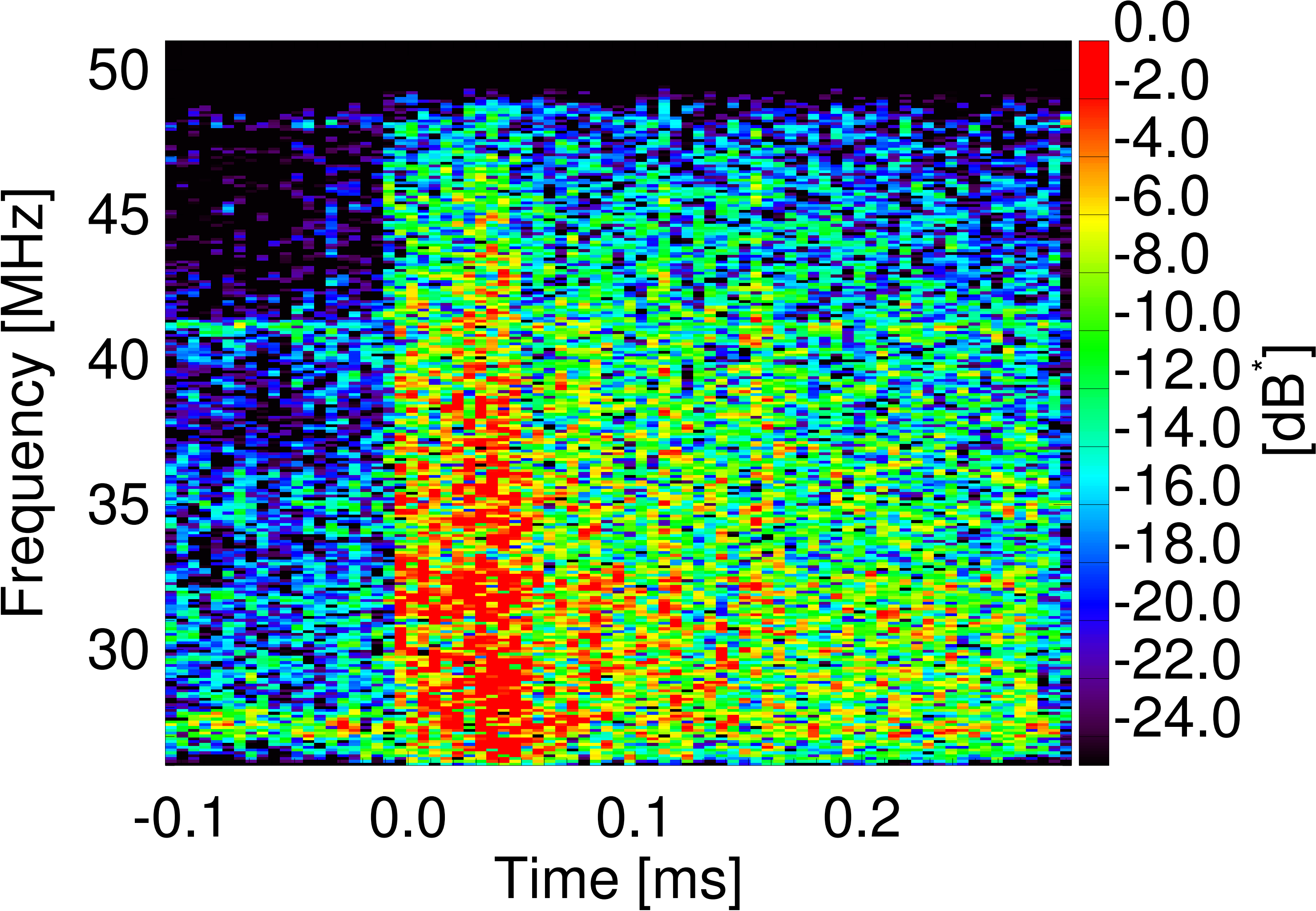


Figure 5.

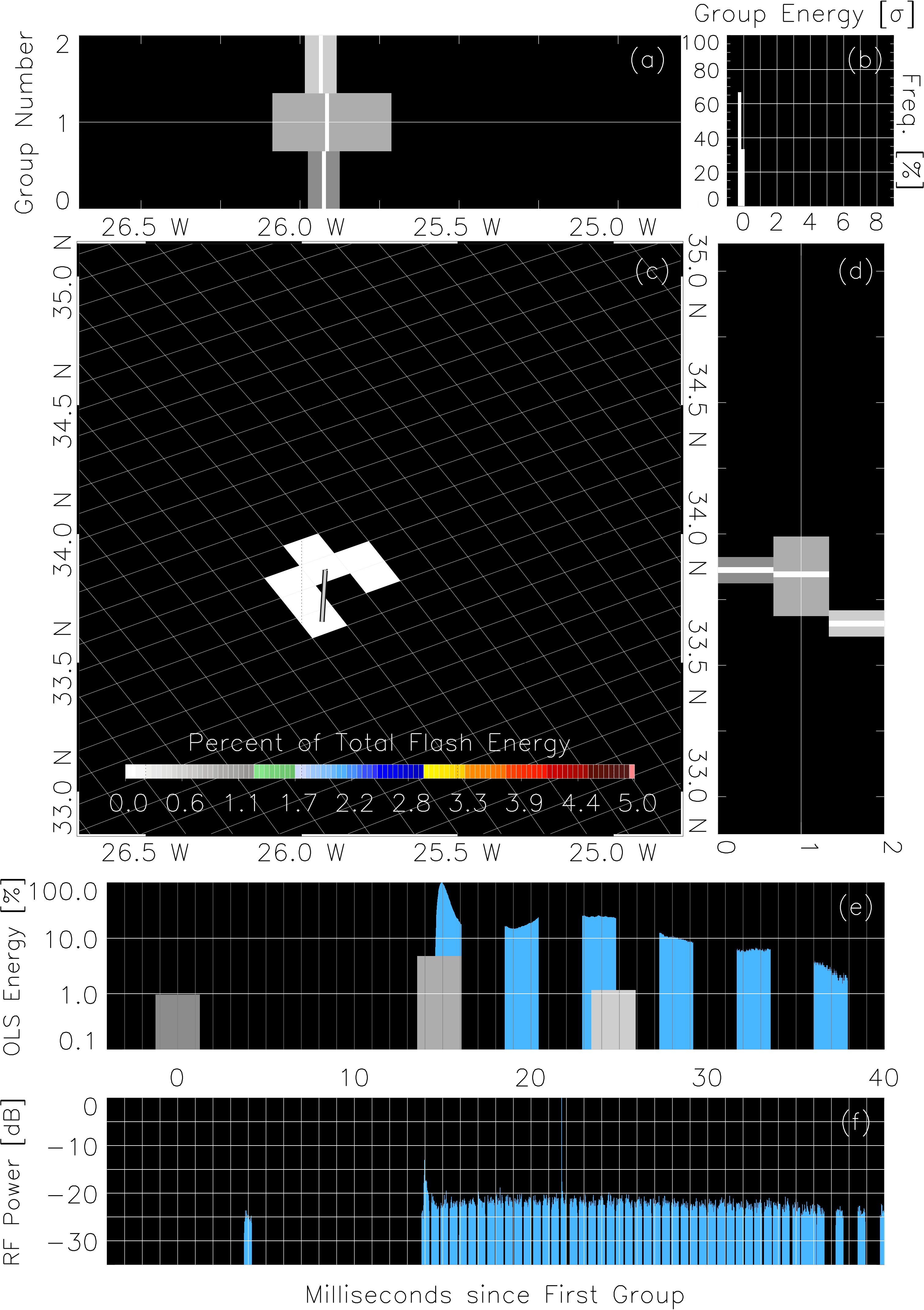


Figure 6.

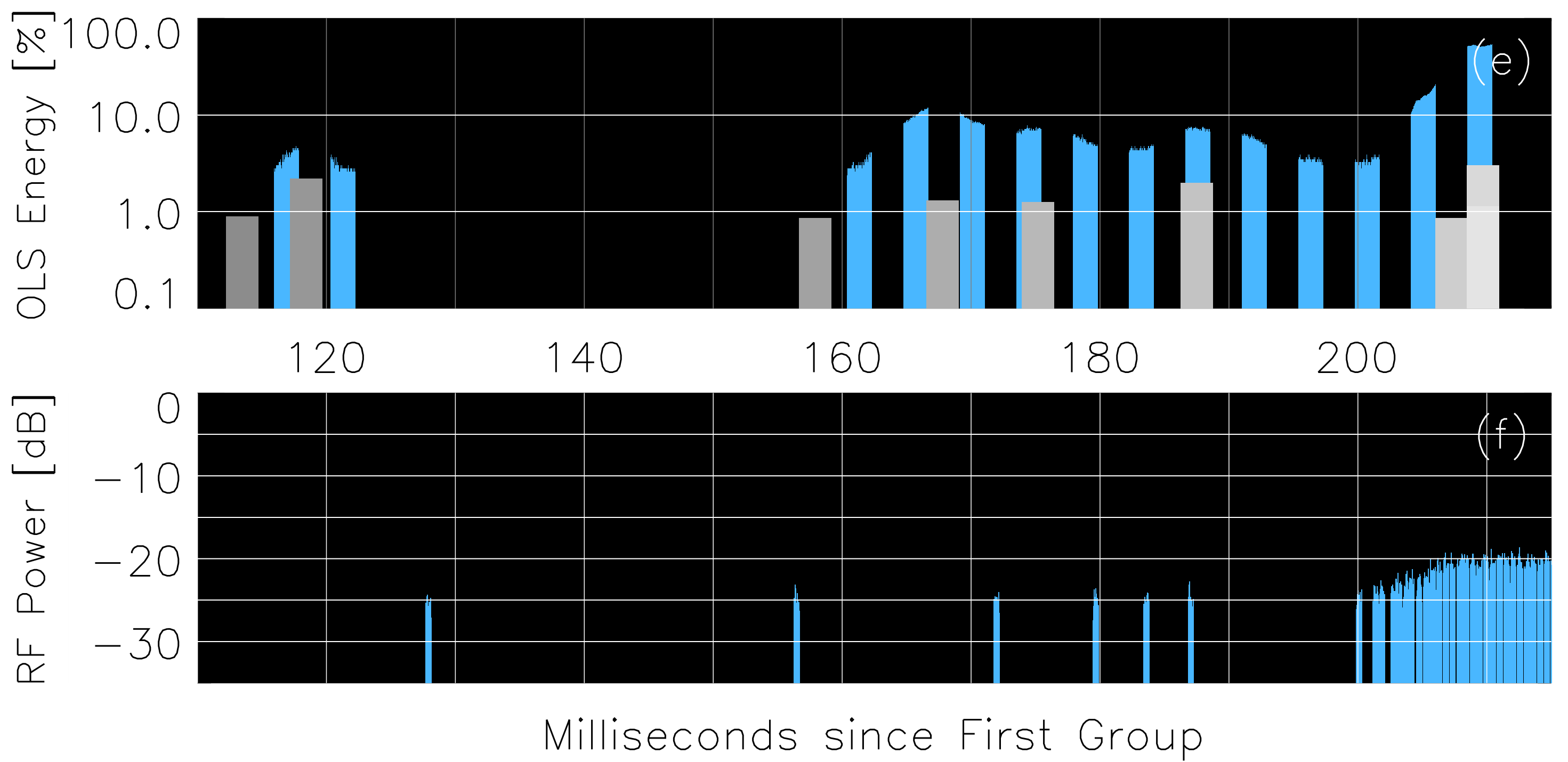
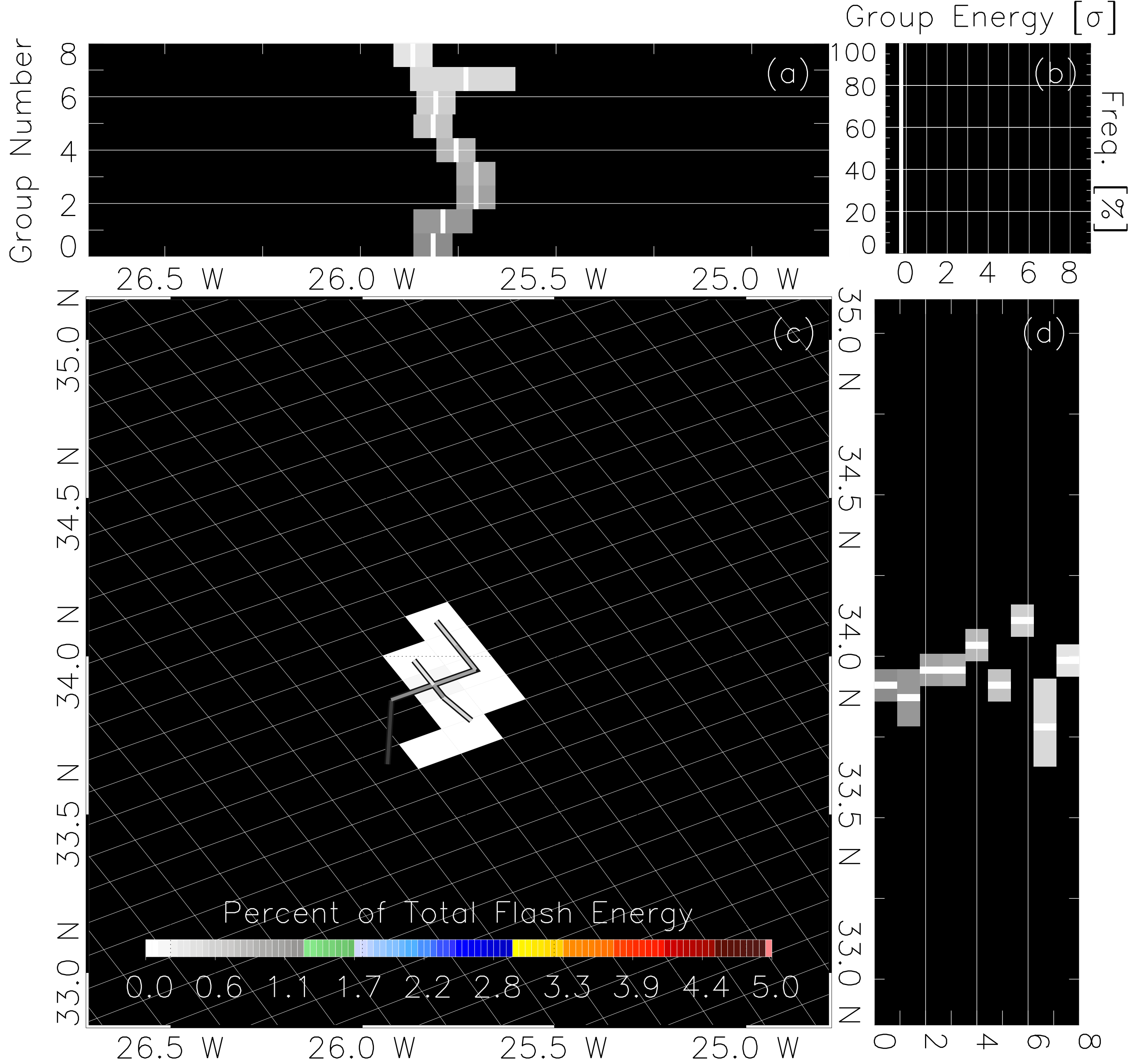


Figure 7.

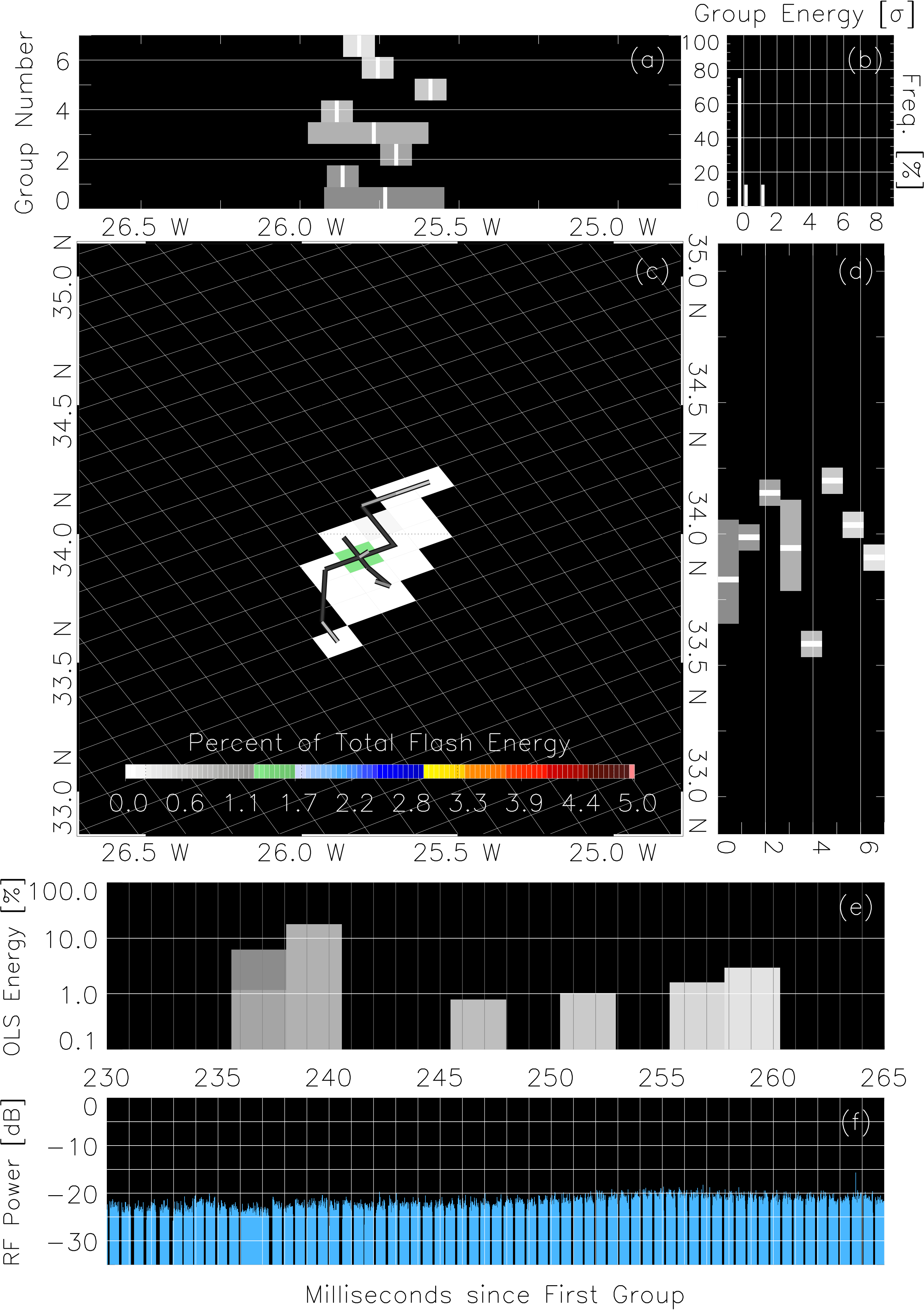


Figure 8.

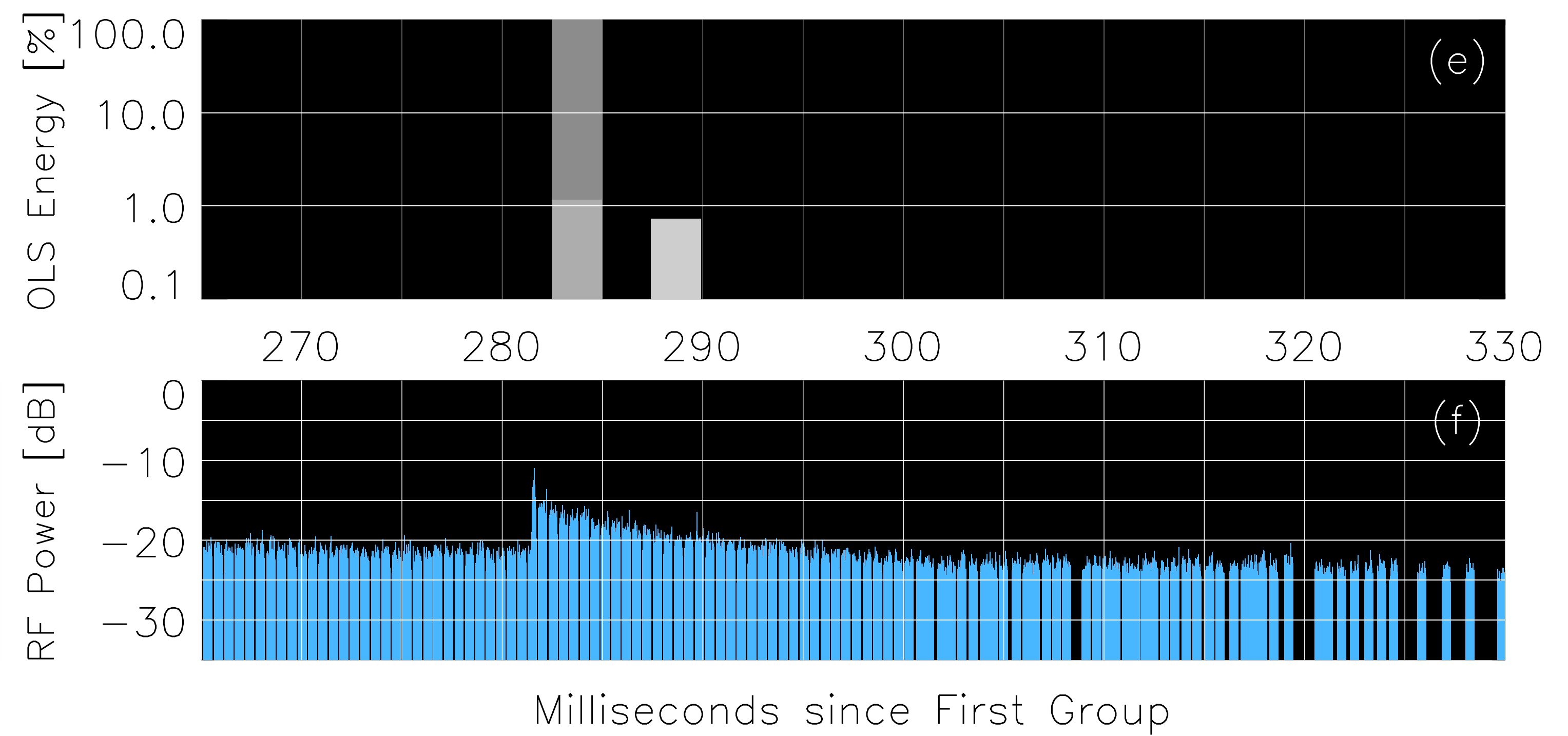
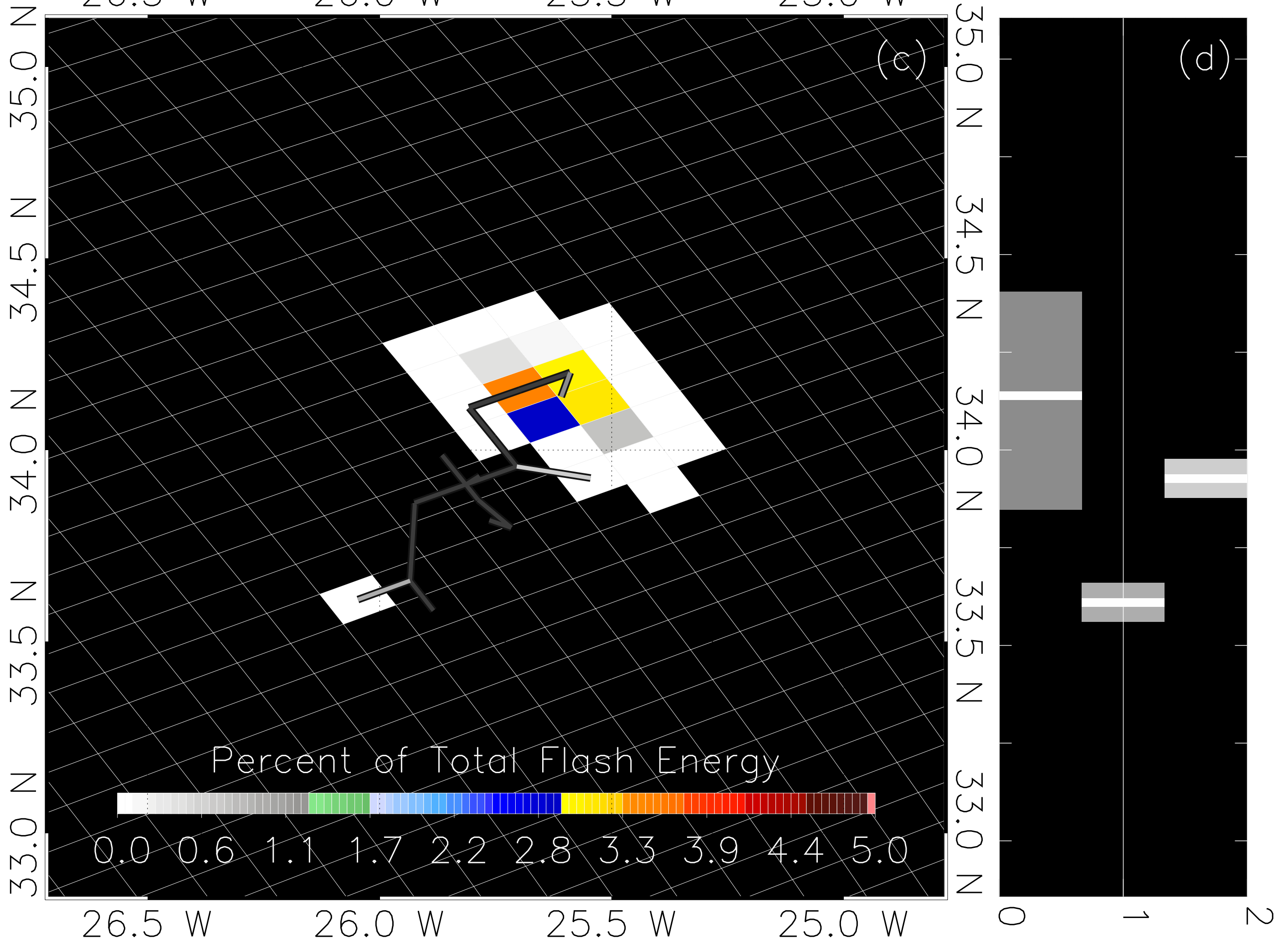
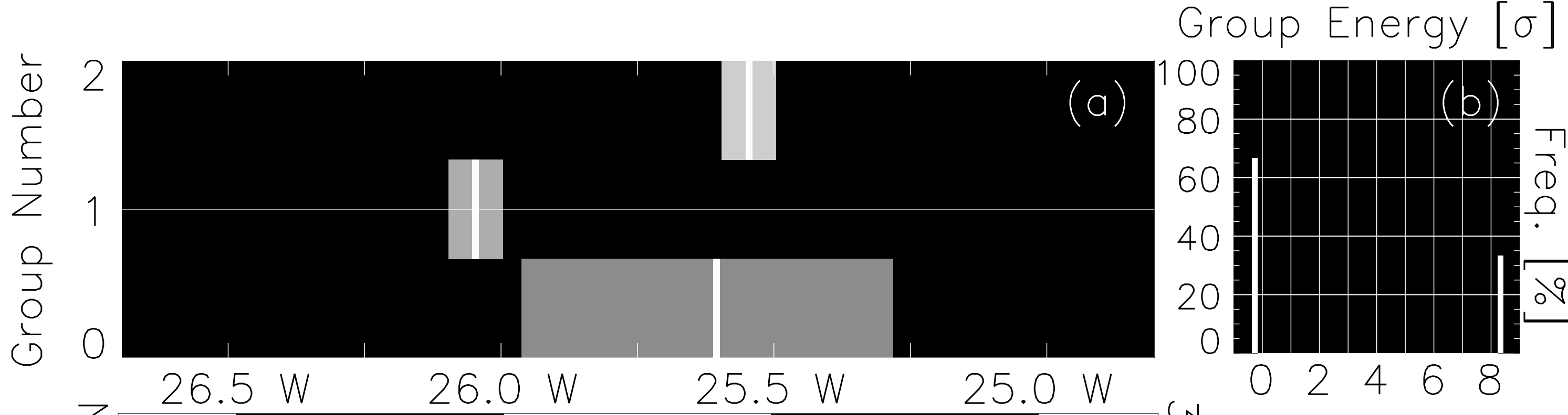


Figure 9.

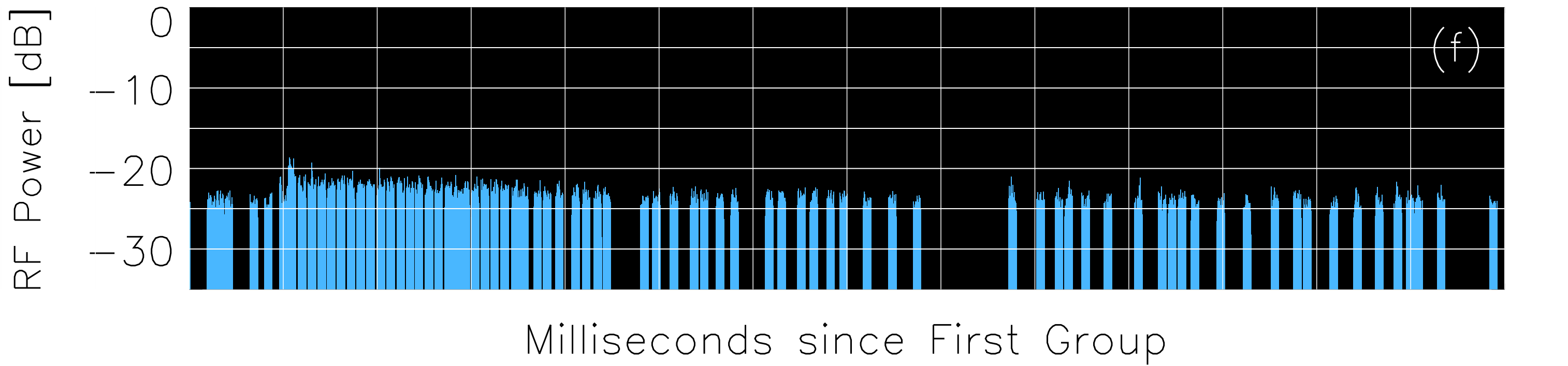
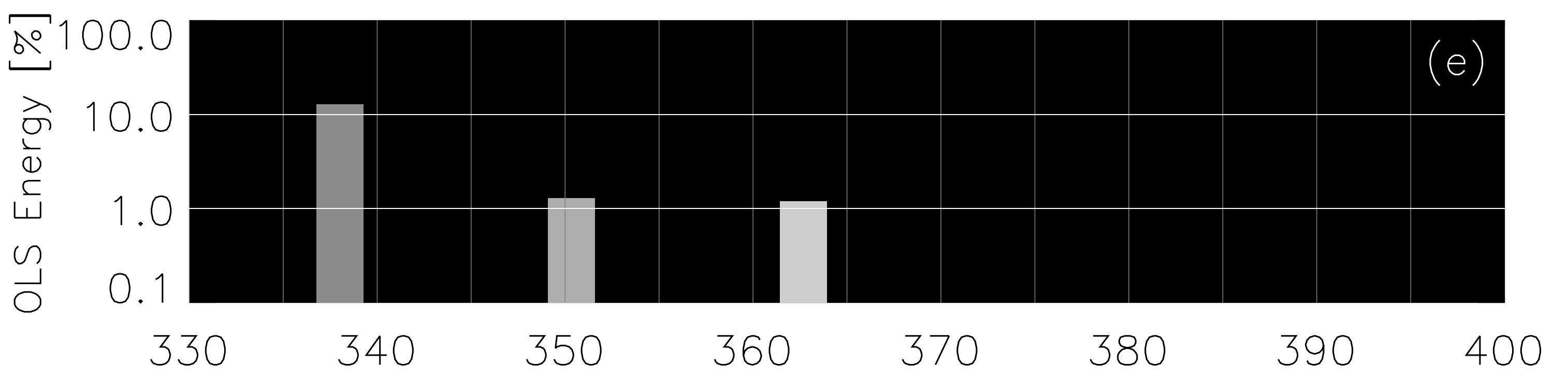
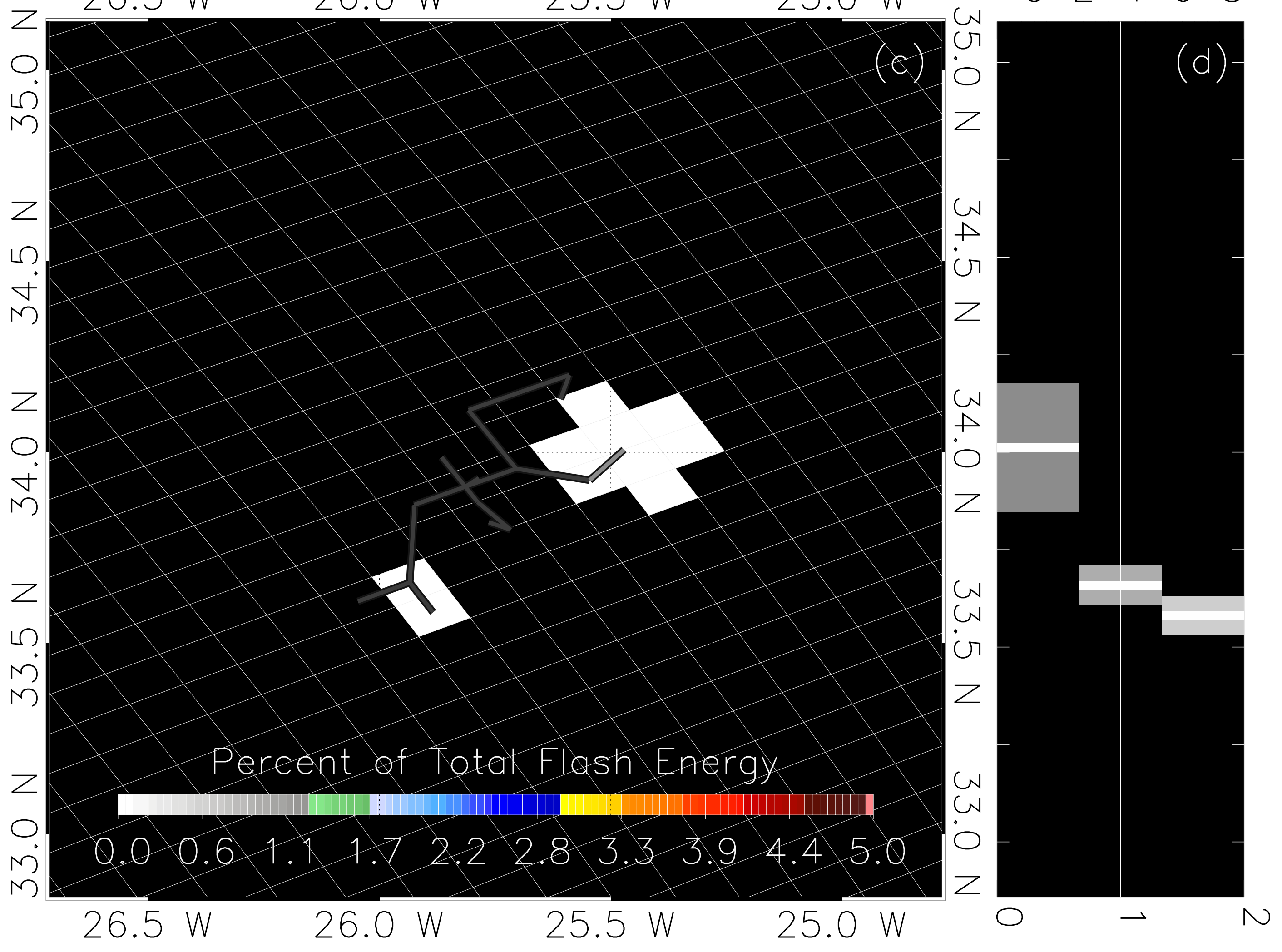
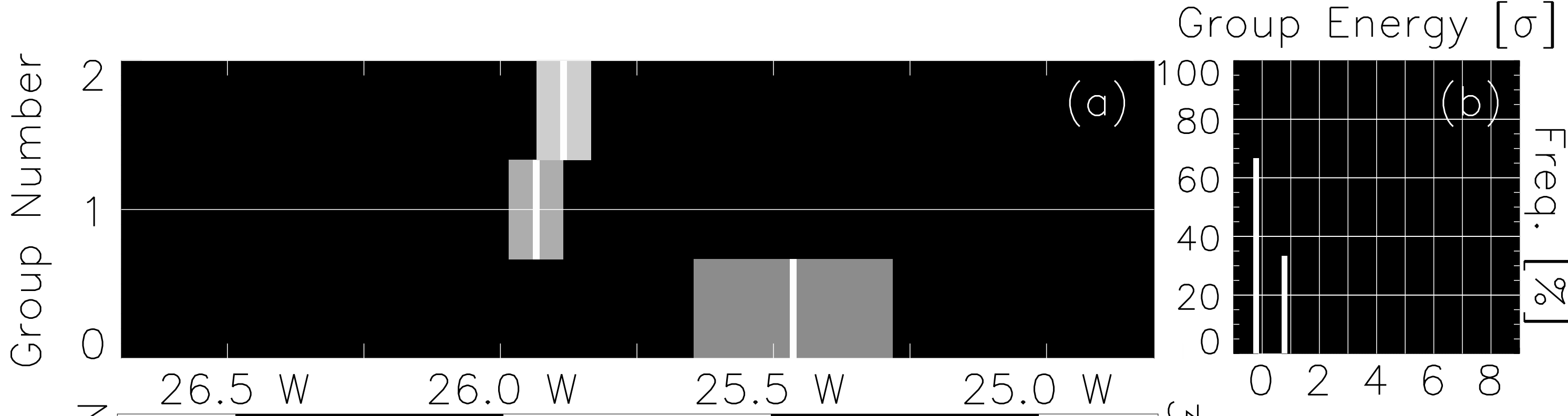


Figure 10.

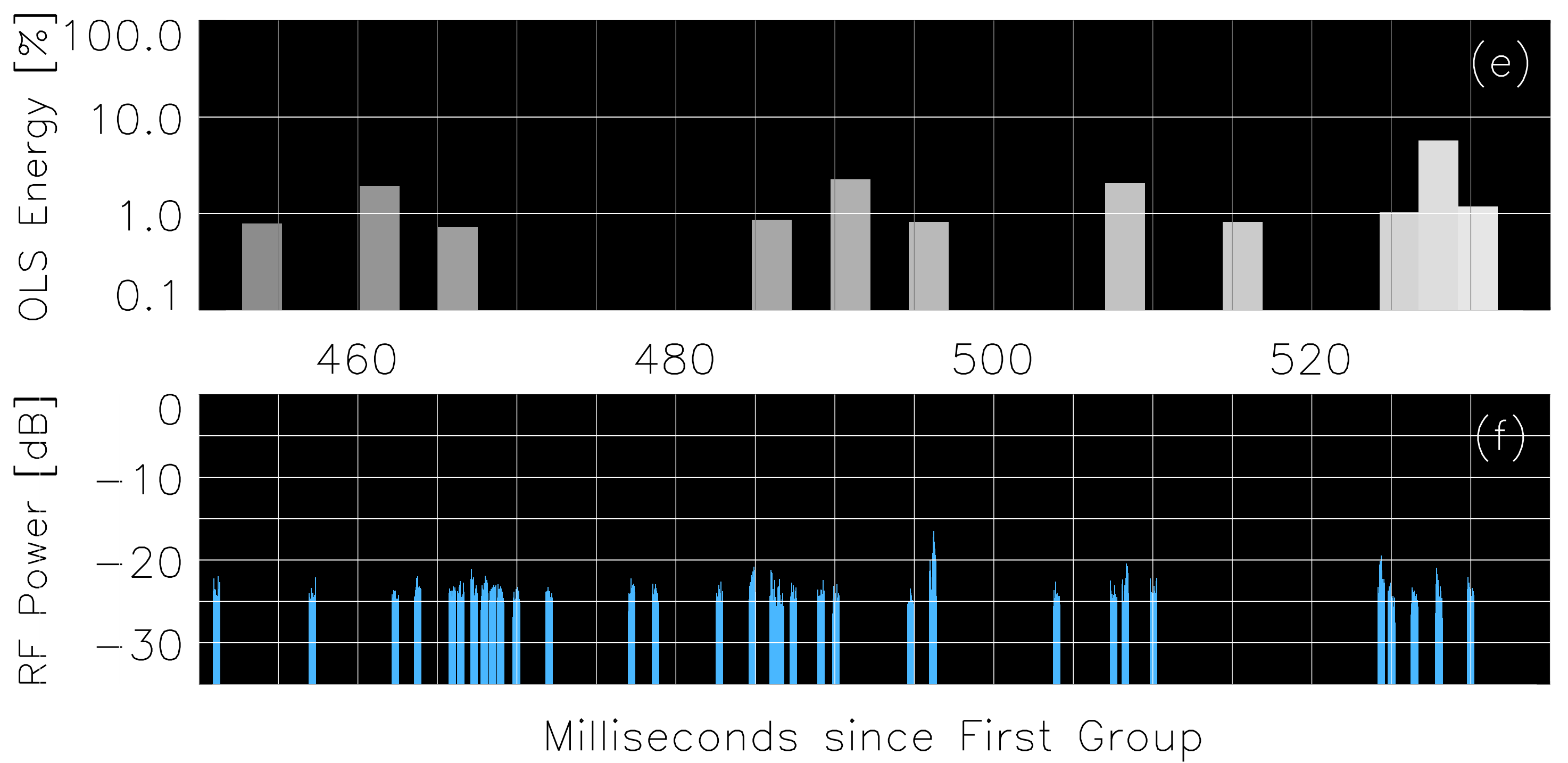
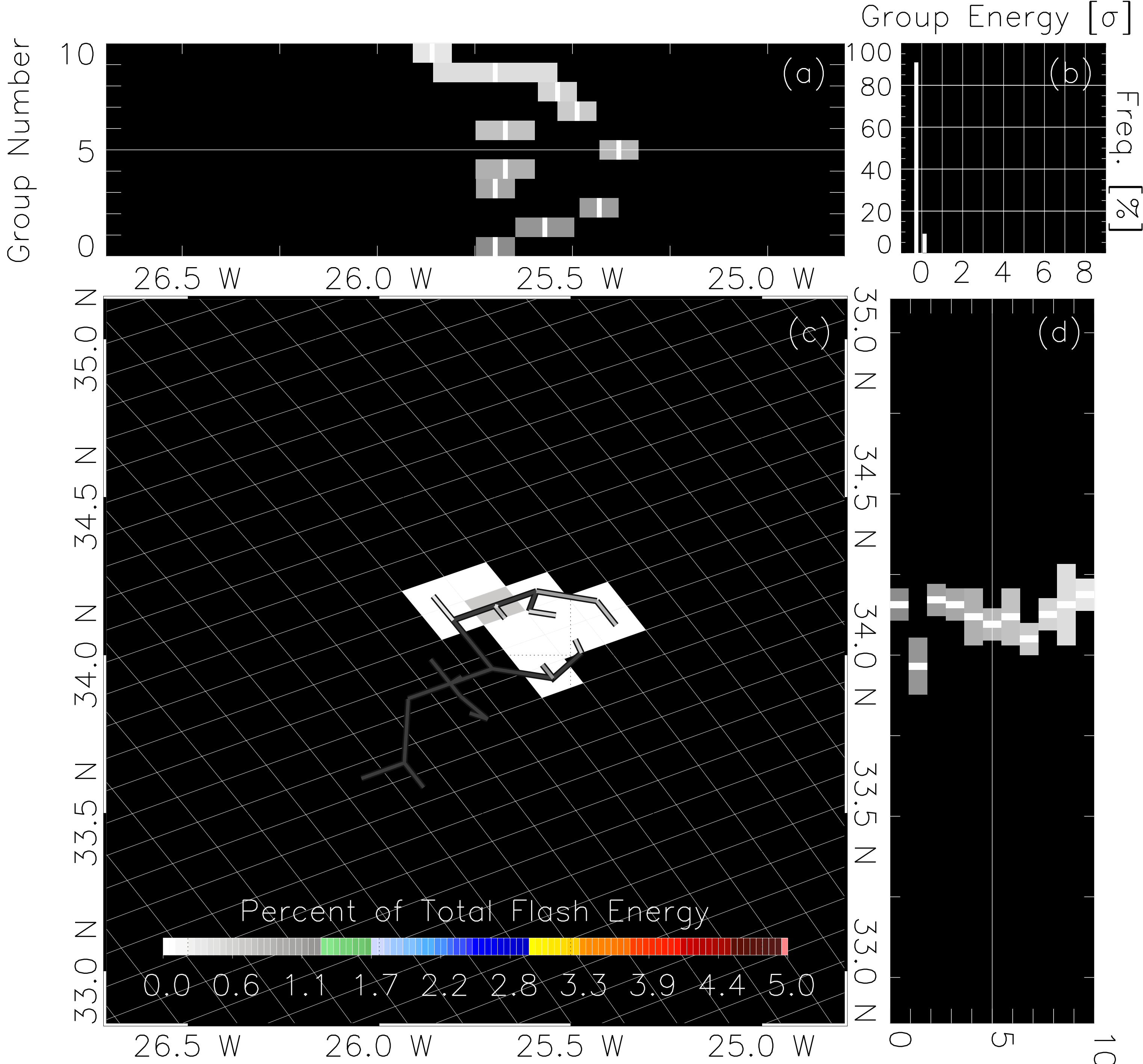


Figure 11.

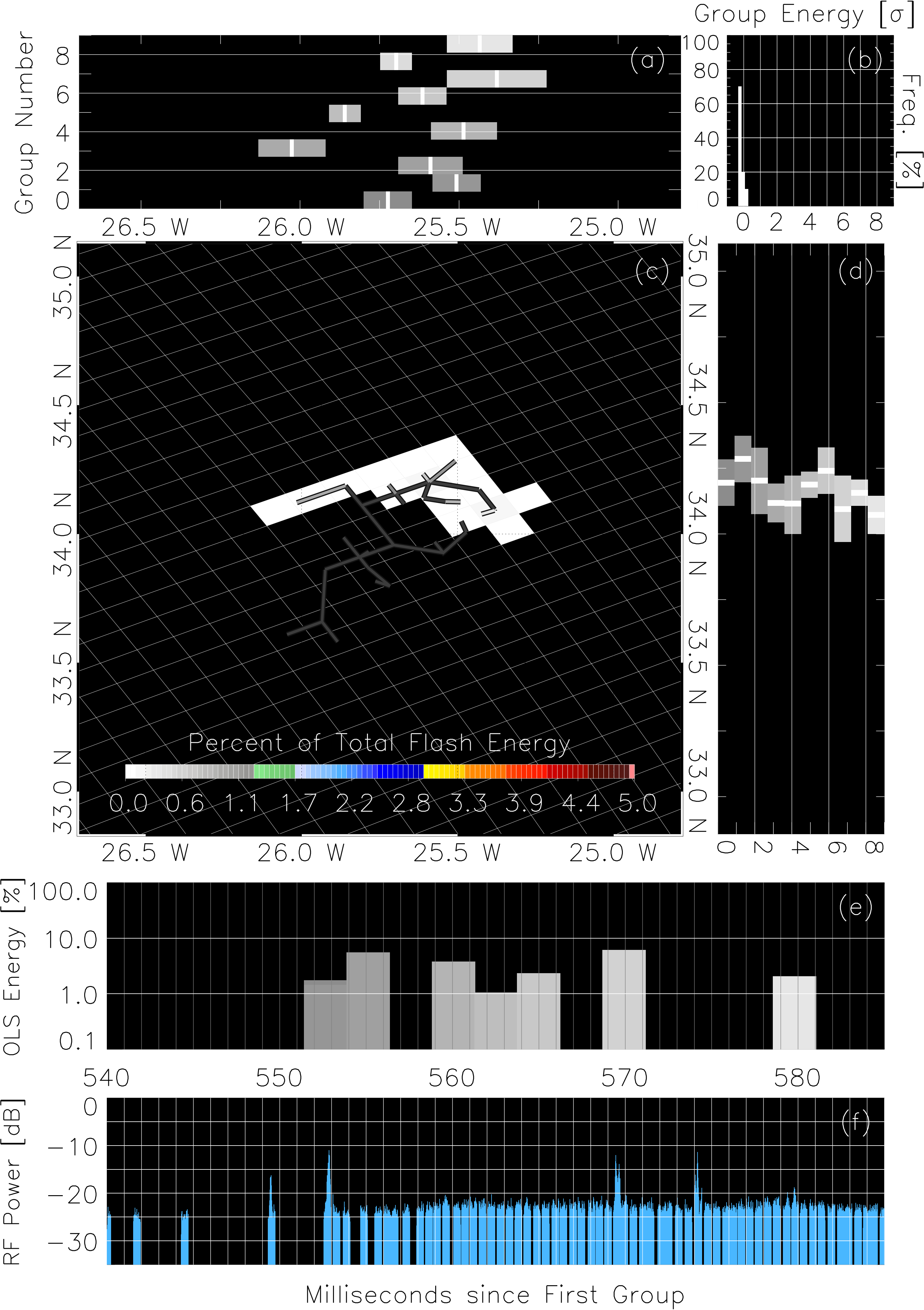


Figure 12.

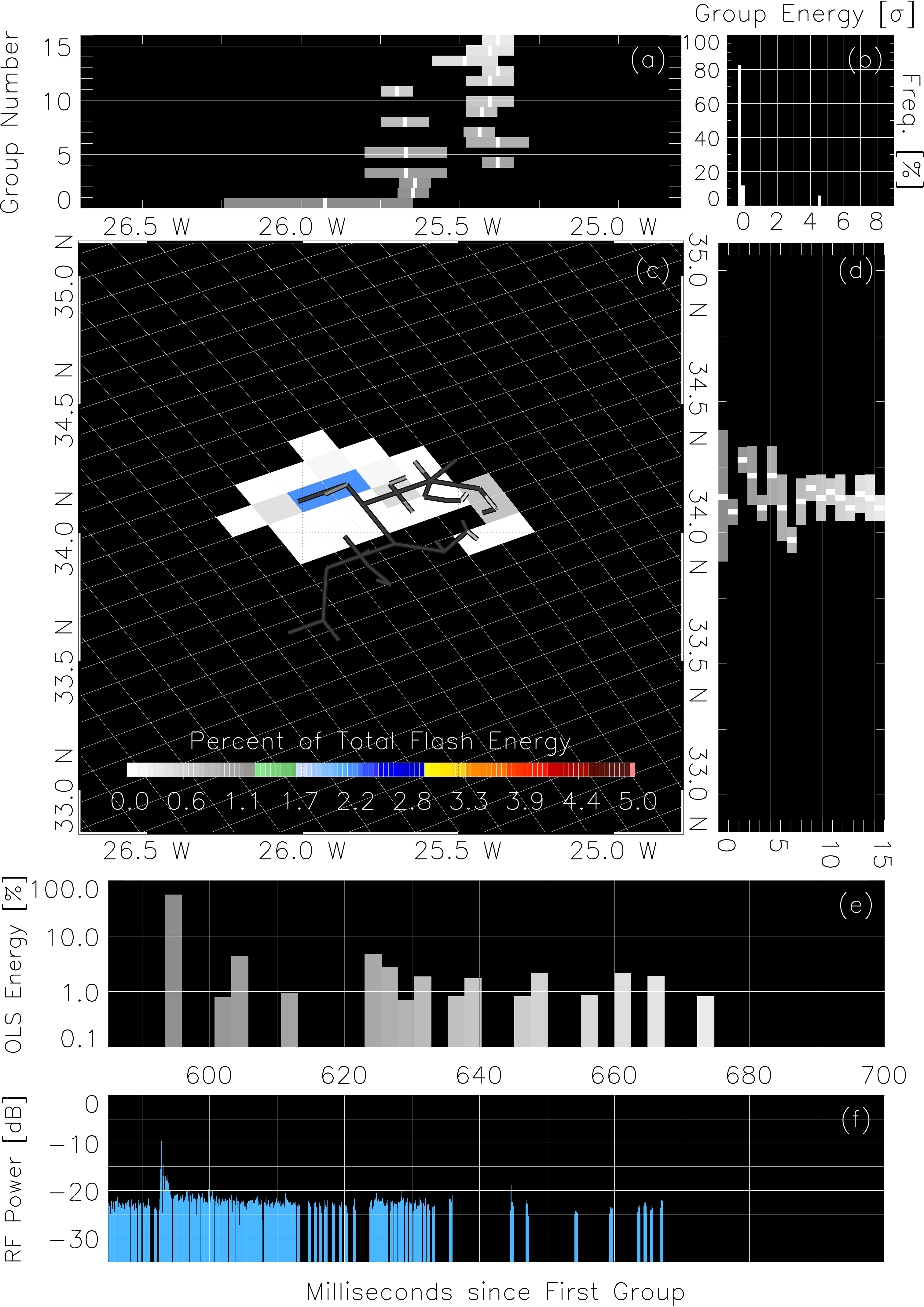


Figure 13.

